EcNikA, a versatile tool in the field of artificial metalloenzymes

Caroline Marchi- Delapierre, Christine Cavazza, Stéphane Ménage

EcNikA, a versatile tool in the field of artificial metalloenzymes

Caroline Marchi-Delapierre, Christine Cavazza, Stéphane Ménage *

Univ. Grenoble-Alpes, CNRS, CEA, IRIG, Laboratoire de Chimie et Biologie des Métaux, 17 rue des Martyrs, F-38054 Grenoble, Cedex, France; e-mail: stephane.menage@cea.fr

Graphical abstract:

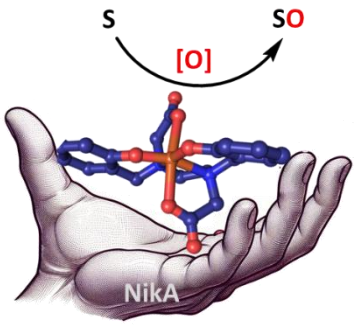

Synopsis: NikA protein scaffold: a helping hand for efficient oxidation catalysis by artificial Fe and Ru metalloenzymes.

Highlights:

- Combining an artificial active site with NikA, an *E. coli* nickel transport protein.
- The protein scaffold decouples the activity of the artificial active site.
- Compared to in-solution conditions, the protein scaffold stabilizes ligand topology.
- An *in cristallo* approach leads to greater stabilization than the in vitro approach.
- Reaction mechanisms are accessible thanks to X-ray crystallography.

Abstract: This review describes the multiple advantages of using of *Ec*NikA, a nickel transport protein, in the design of artificial metalloenzymes as alternative catalysts for synthetic biology. The

rationale behind the strategy of artificial enzyme design is discussed, with particular emphasis on *de novo* active site reconstitution. The impact of the protein scaffold on the artificial active site and thus the final catalytic properties is detailed, highlighting the considerable aptitude of hybrid systems to catalyze selective reactions, from alkene to thioether transformations (epoxidation, hydroxychlorination, sulfoxidation). The different catalytic approaches – from *in vitro* to *in cristallo* – are compared, revealing the considerable advantages of protein crystals in terms of stabilization and acceleration of reaction kinetics. The versatility of proteins, based on metal and ligand diversity and medium/physical conditions, are thus illustrated for oxidation catalysis.

Keywords: catalysis, oxidation, artificial metalloenzymes, iron, ruthenium, Cross-linked enzyme crystals.

Introduction.

Biocatalysis represents the keystone for the expansion of synthetic biology, driven by the need for sustainable chemistry. Synthetic biology should surpass synthetic chemistry in the future if it can provide the same diversity as chemical synthesis.[1] More particularly, there is a great dynamic for using natural metalloenzymes and adapting them to a targeted purpose such as C-H activation, C-C bond formation, and many more.[2] Nevertheless, the diversity of metalloenzymes is far from that of man-made catalysts. The search for artificial systems that can deliver all kinds of products is very active, and abiotic reactions have now been reached, thanks to directed evolution or related processes applied to natural enzymes. For example, in rare cases, it was demonstrated that abiotic reactions can be driven by the kinetic parameters of natural enzymes, for example after switching the metal ion and performing several amino acid substitutions in a natural CytP450.[3] In addition, an anti-Markovnikov oxidation of alkenes by a CytP450 variant was obtained by another beneficial-multiple-mutation, some at considerable distance from the active site.[4] More recently, the use of artificial intelligence has led to a major breakthrough in the field of artificial metalloenzymes (ArMs) for this purpose.[5]

Another strategy for the construction of ArMs pushes back the limits of the possible, in particular in the field of oxidation catalysis. This strategy consists in mimicking the structural parameters of natural metalloenzymes to imitate their enzymatic characteristics: chemo, regio(enantio)selectivity, and mild reaction conditions, one of the key requirements for sustainable chemistry. Accordingly, reaction selectivity should be reproduced from a common catalytic pathway (involving second-sphere interactions),[6] and substrate orientation should be guided by creating an appropriate binding site.[7] Several approaches have been developed ranging from switching metals (mainly in heme proteins) – derived from natural enzymes – to rational, *de novo* protein design.[8] The binding domain is strongly affected by the various interactions between the metal complexes and the protein scaffolds. Several types of interactions have been demonstrated, from salt bridges to Π stacking.[9] For example, the importance of the second coordination sphere is nicely illustrated by the work of O. Shoji,[10] where a decoy molecule, analog of the hemoprotein's substrate, is used to activate the artificial enzyme.

Nevertheless, one particular means to create these hybrids has attracted our attention: *de novo* active site reconstitution. With this method, an inorganic or organometallic catalyst is embedded within a protein scaffold. This strategy represents a bridge between organometallic (inorganic) chemistry and biocatalysis, with both fields contributing to the originality of the final activity.

Indeed, the resulting hybrid contains an artificial active site, which controls the nature of the reaction, and a protein scaffold, which controls reaction selectivity. Moreover, the control of the activity also depends on how the artificial active site interacts with the protein backbone, including through dative or supramolecular interactions and covalent bonds (Figure 1). The obvious methodology involves possible interactions between an amino acid residue and a coordination site in the metal complex. This interaction is nicely illustrated by the insertion of Co and Mn salen complexes into myoglobin or CP450s scaffolds, to create metalloenzymes that can bind a heme prosthetic group with a histidine or cysteine amino acid residue, respectively.[11] Another elegant methodology, known as the *trojan horse* strategy, exploits high-affinity ligand/protein interactions. As the biotin/avidin system holds the record for the affinity between substrate and host, (strept)avidin/biotin technology has been used to generate powerful ArMs, by decorating the metal complex with a biotin molecule.[12]

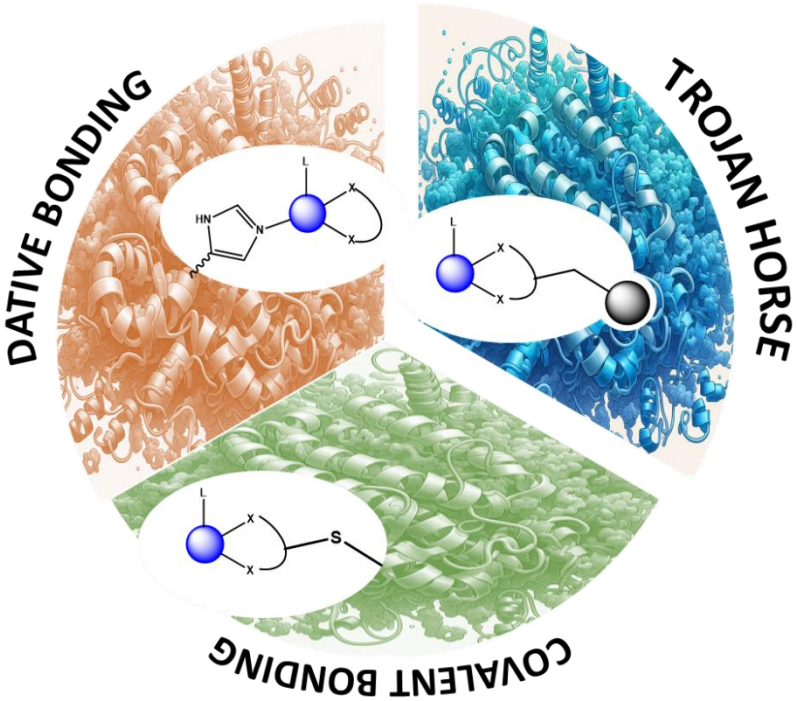

Figure 1. Different modes of metal complexes insertion to design an ArM. Brown: Dative coordination with an unsaturated metal complex; Blue: supramolecular coordination using a high-affinity anchor; Green: covalent bonding of the ligand.

Furthermore, the main asset of *de novo active site reconstitution* is how easy it is to produce a target reactivity by adding the appropriate complex and searching for the parameters controlling

selectivity. This last aspect is often achieved by site-directed mutagenesis of the host protein. Interestingly, the search for selectivity parameters also helps to determine the exact role of each part of the hybrid. Indeed, the main challenge is to increase efficiency through the association, thanks to supramolecular interactions controlling the active site's electronics and the binding of the substrate or various reactants, generating selectivity. A growing number of hybrid artificial oxygenases are now available for epoxidation, sulfoxidation, dihydroxylation, peroxidation, and amine, water, alcohol and catechol oxidations.[7d] Nevertheless, compared to natural enzymes, optimization of these artificial enzymes is more challenging. For instance, in the directed evolution methodology, the active site must be inserted in each round of evolution, which creates an obstacle for high-throughput processes.[1a] Finally, an alternative covalent variant of ArMs is drawn from biorthogonal fundamentals. For example, several reports describe attempts to induce the Michael addition of a maleimide fragment of the metal ligand to a cysteine residue.[13] Methods to incorporate non-natural amino acids have also been successful, as exemplified by the insertion of a bipyridine moiety into LmrR.[14]

The main challenge for ArMs design relates to the sustainability of these hybrids. As a common answer to this challenge in chemistry, the heterogeneous version of *in vitro* enzymes should help to reach high standards of biocatalysis. This strategy should also ensure easy recovery of the products, and compatibility with a large range of solvents. Several strategies, from encapsulation (in polymer matrix, metal organic frameworks (MOF), liposomes, or inverse micelles) to surface-immobilization (nanoparticles in particular), have gained attention and helped to develop catalysis in organic media.[15] Each of these strategies has drawbacks that affect the biocatalyst's efficiency, from the denaturation of the enzyme when attached at multiple points on a support, to limited substrate diffusion when the enzyme is entrapped in a polymer matrix. As an alternative to cross-linked enzyme aggregates, the Cross-Linked Enzyme Crystals (CLEC) strategy has attracted our attention (Figure 2).[16] Beyond the well-known difficulties of crystallogenesis, this strategy has multiple assets: i) it provides the highest accessible concentration of enzymes in solid form; ii) ensures enzyme integrity; iii) can be used to determine 3D structures by X-ray crystallography, and iv) makes it possible to use solvent channels for substrate diffusion. The CLEC methodology was initially fully developed with natural enzymes,[17] and it has only recently been optimized for ArMs by our group.

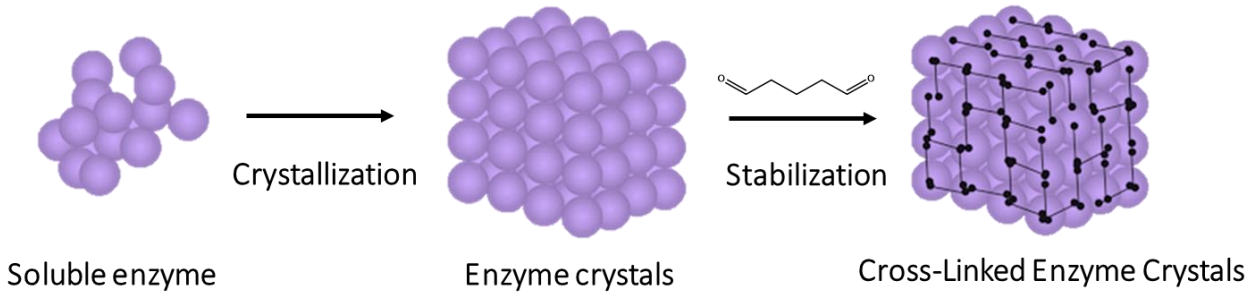

Figure 2. Illustration of the Crossed-Linked Enzyme Crystals methodology.

The emergence of novel ArMs as alternatives to natural metalloenzymes has pushed us to review the recent breakthroughs in this field through the prism of our contribution, using *Ec*NikA from *Escherichia coli* (*Ec*NikA) as the protein scaffold. We undertook to associate *Ec*NikA, a nickel transport protein, with inorganic complexes that were, in most cases, capable of moderate catalytic oxidation in organic solvents through homogeneous catalysis. We selected the design of ArMs based on the supramolecular interactions controlling their anchoring to develop several artificial oxygenases. This review details the knowledge accumulated over the last 15 years on this topic, highlighting the role of the *Ec*NikA protein. After a general description of the *Ec*NikA scaffold and the origins of the project, we present several structural parameters that influence the reactivity of biohybrids, providing hints for future design methods and hope for future applications.

1. *Ec*NikA "history": a host protein for natural Ni import

In bacteria, Ni(II) is transported through the cytoplasmic membrane by a variety of high-affinity uptake systems.[18] Among them, ABC-importers are comprised of five components: two channel-forming transmembrane proteins (TMPs) and two nucleotide-binding proteins (NBP).[19] The fifth component is an extra-cytoplasmic solute-binding protein (SBP), called Ni-BP in Ni(II) ABC-type importers. In gram-negative bacteria, such as *E. coli*, the Ni-BP is present in the periplasm. It is the initial Ni(II) receptor, and the major determinant of importer specificity and efficiency.[20] For 15 years, we have been designing ArMs using the Ni-BP from *E. coli*, *Ec*NikA, as host protein. *Ec*NikA (accession code: P33590) is a 56-kDa protein (502 amino acids in its mature form) with a 22-amino acid peptide leader that directs the protein toward the bacterial periplasm. When deprived of this signal sequence, *Ec*NikA can be overproduced in the *E. coli* cytoplasm with yields reaching 100 mg of pure apo-protein per L of culture.

*Ec*NikA has two lobes (domains I and II) connected by a hinge region that closes upon ligand

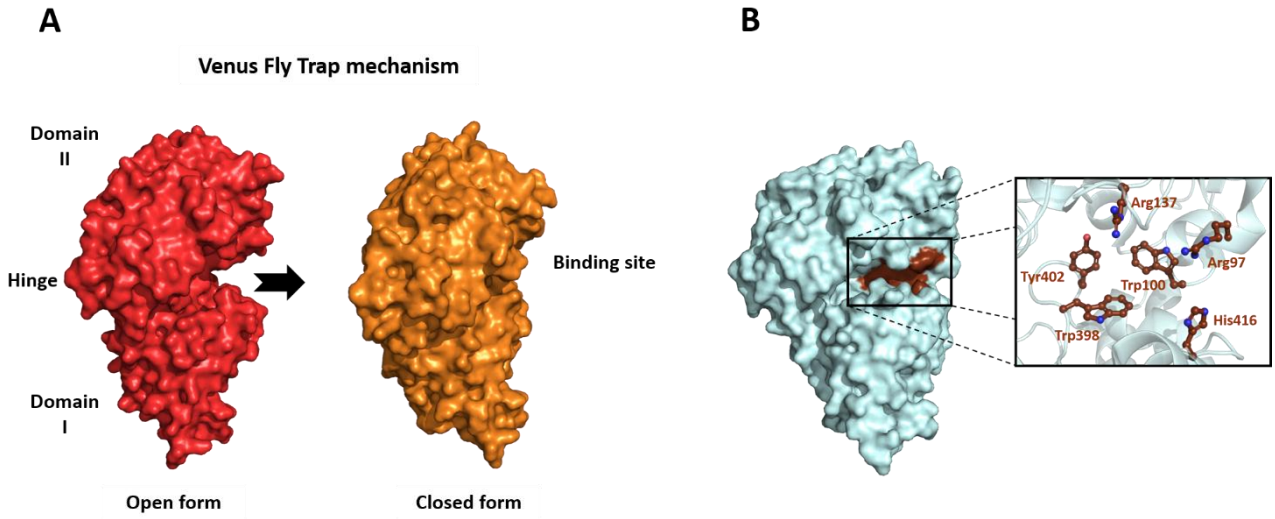

binding through a conserved "Venus Fly-trap" mechanism found in all SBP (Figure 3A).[21]

Figure 3. The Ni-binding protein NikA from *E. coli*. A) The Venus Fly-trap mechanism between the unliganded form (PDB code: 1UIU) and the Nickel-bound form (PDB code: 4I8C). B) X-ray structure of *Ec*NikA (PDB code: 1ZLQ). The residues constituting the binding site are colored in brown. A close-up of the binding site is shown in the inset.

The two major *Ec*NikA states observed are an unliganded open form and a ligand-bound closed form. In 2003, Heddle and collaborators[22] provided the first structural descriptions of both open and closed forms. The metal-free open form crystallized in space group $P3_2$ as triangular prims. Conversely, in the presence of Ni(II), metal-bound *Ec*NikA was visualized as orthorhombic crystals in the $P2_12_12_1$ space group. The metal-binding site was identified and described as a pocket with numerous aromatic and arginine residues (Figure 3B). At the time, the authors proposed that the cavity hosted a Ni-$(H_2O)_5^{2+}$ species. Later, in 2005, Cherrier *et al.*[23] solved the X-ray structure of *Ec*NikA in complex with Fe(III)-EDTA$(H_2O)^-$ (Figure 4A). Unexpectedly, when EDTA is used as metal chelator throughout purification, instead of obtaining the expected open apo-form, *Ec*NikA binds metal-EDTA with high affinity to form a ligand-bound closed state. This result suggested that a metal-EDTA complex, instead of a pentahydrated Ni(II), was also present in the original structure proposed by Heddle *et al.* in 2003.[22] In this configuration, EDTA is stabilized in the binding pocket by supramolecular interactions, and the iron ion does not directly interact with the protein. Consequently, characterization of the *Ec*NikA binding site strongly suggests that a metallophore (or more precisely a nickelophore) is required to bind Ni(II) to the protein. A few years later, Chivers and colleagues[24] demonstrated the role played by L-Histidine in Ni(II) import in *E. coli*. This

demonstration was followed by the structural characterization of *Ec*NikA in complex with Ni(L-His)$_2$ (Figure 4B), which was proposed to be the physiological Ni(II) complex imported by the ABC transporter in *E. coli.* Ni(L-His)$_2$-bound *Ec*NikA yielded hexagonal crystals in the P62 space group, corresponding to a closed conformation of the protein (Figure 4C).[25]

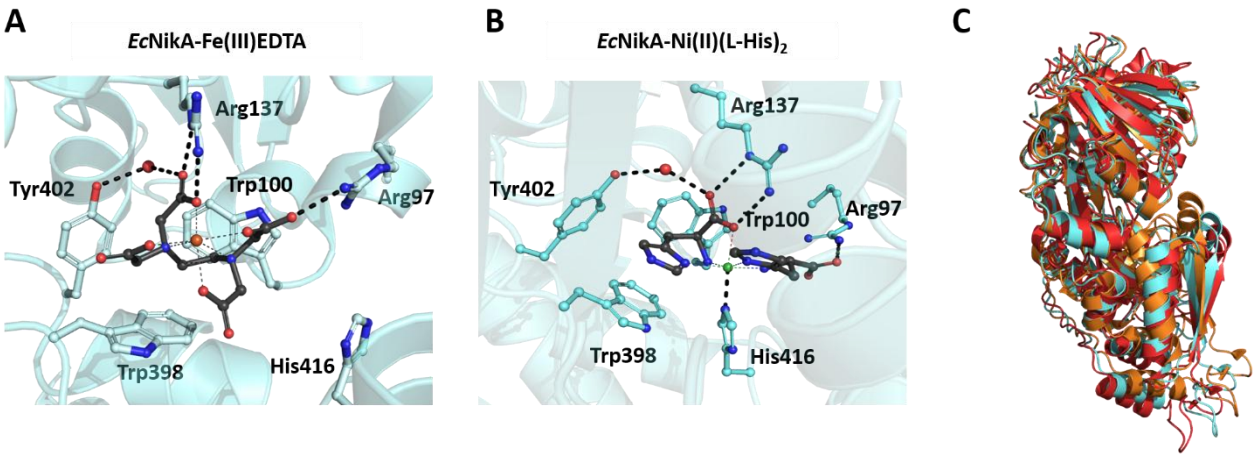

Figure 4. A) Fe(III)-EDTA binding site. The Fe atom is depicted as a red sphere; EDTA is illustrated in gray (PDB code: 1ZLQ). B) Ni(L-His)$_2$ binding site. The nickel atom is depicted as a green sphere. The two free L-His are depicted in gray (PDB code: 4I8C). Surrounding amino acids are illustrated by cyan sticks. C) Superimposition of the crystal structure of the open unliganded form (red, PDB code: 1UIU), the Fe-EDTA-bound form (cyan) and the closed Ni(L-His)$_2$-bound conformation (orange).

In the Ni(II)-bound conformation, a significant conformational change occurs compared to the Fe(III)EDTA-bound form, bringing His416 within binding distance of the Ni(II). The nickel N_5O coordination involves four nitrogen atoms from the imidazole rings and the amine groups of the two free histidines (His1 and His2), the carboxylate group of His1, and – as the only direct metal-protein contact – one nitrogen atom from the imidazole ring of His416 from *Ec*NikA (Figure 2B). Compared to free Ni(L-His)$_2$ in solution, the imidazole ring of His416 replaces the carboxylate group of His2, which no longer interacts with the nickel ion, leading to rearrangement of the complex within the protein.

A good description of ligand-protein interactions provides valuable input for ArM designers. In the case of *Ec*NikA, once its X-ray structure had been determined it became possible to create novel ArMs by anchoring EDTA-like complexes inside its binding site. X-ray structures revealed that both metal-EDTA complexes and Ni(L-His)$_2$ bind to *Ec*NikA *via* a salt bridge between Arg137 and a carboxylate group. We therefore considered the presence of at least one carboxylate group in the ligand as an essential requirement for its binding to *Ec*NikA. A second carboxylate group can also interact with Arg97 to reinforce the stability of the complex inside the protein cavity. To take this a step further, we carried out a detailed characterization of the factors determining the interaction

between artificial ligands and *Ec*NikA.[9] A series of "ML@NikA" hybrids have now been thoroughly characterized by X-ray crystallography, biophysics and quantum chemistry. The ligands were varied in terms of charge, geometry, aromaticity, and size. The study confirmed the central role of Arg137 in the stabilization of ligands *via* its interaction with a carboxylate group. Its binding is reinforced by interaction with a structural water molecule that also interacts with Tyr402. As the *Ec*NikA binding pocket is positively charged, the number of negative charges in the bound complex also significantly influences the affinity (with K_D ranging from 75 nM for Ni(L-His)$_2$, 2.5 µM for Fe(III)-EDTA, to about 60 µM for positively-charged complexes). In addition, the geometry of the ligand plays an important role, helping it to fit the protein cavity. For example, planar complexes such as metal-salen cannot bind to *Ec*NikA owing to steric hindrance. When present, aromatics can form π-π stacking interactions with surrounding amino acids (Trp100, Trp398, His416 and Tyr402) (Figure 1B). Finally, we demonstrated the crucial role of weak interactions in the stabilization of metal complexes in the *Ec*NikA cavity. The presence of several π-acceptor residues in the binding site allows the creation of a network of CH/π interactions which play a determinant role.

Our knowledge of *Ec*NikA was clearly an asset in our choice of protein scaffold. Besides the study of *Ec*NikA hybrids in solution, we took advantage of the fact that Fe^{III}EDTA@NikA crystals can readily be obtained in a reproducible way for further studies. In our work, the strategy was to produce orthorhombic Fe^{III}EDTA@NikA crystals, which were subsequently incubated with a large excess of the desired complex. This soaking led to the replacement of Fe(IIII)-EDTA inside the NikA cavity, as confirmed by the resolution of the resulting crystal structures.

The availability of crystal structures of "ML@NikA" hybrids made structure-activity studies possible. The structures of "ML" complexes inside the protein cavity provided a detailed view of the metal's geometry and environment, as well as of ligand anchoring. This information is crucial for ligand optimization strategies, to achieve the desired activity and performance. For example, in the case of the **Fe^{Py}LX** series (Chart 1), this approach was decisive. **Fe^{Py}LX** complexes were synthesized as a mixture of several topologies.[26] Initially, when Fe^{III}EDTA@NikA crystals were soaked with **Fe^{Py}L1**, a complex mixture of topologies was present in the binding site. However, the stiffer complex **Fe^{Py}L2** (due to the presence of a cyclohexyl backbone) is only present in either *trans* or *cisβ* topologies in *Ec*NikA molecules present in the asymmetric unit (Figure 5). This selectivity inside the crystal was unexpected, and likely due to the crystal packing creating more or less disorder between the *Ec*NikA molecules, thus favoring the binding of one topology or the other. These results led us to synthesize the dimethyl analog complex, **Fe^{Py}L3**. The crystal structure

of **Fe^{Py}L3**@*Ec*NikA revealed that, in this case, only the *cisß* topology was observed (Figure 5). We were therefore able to obtain a homogeneous catalyst, and to proceed with catalytic studies.

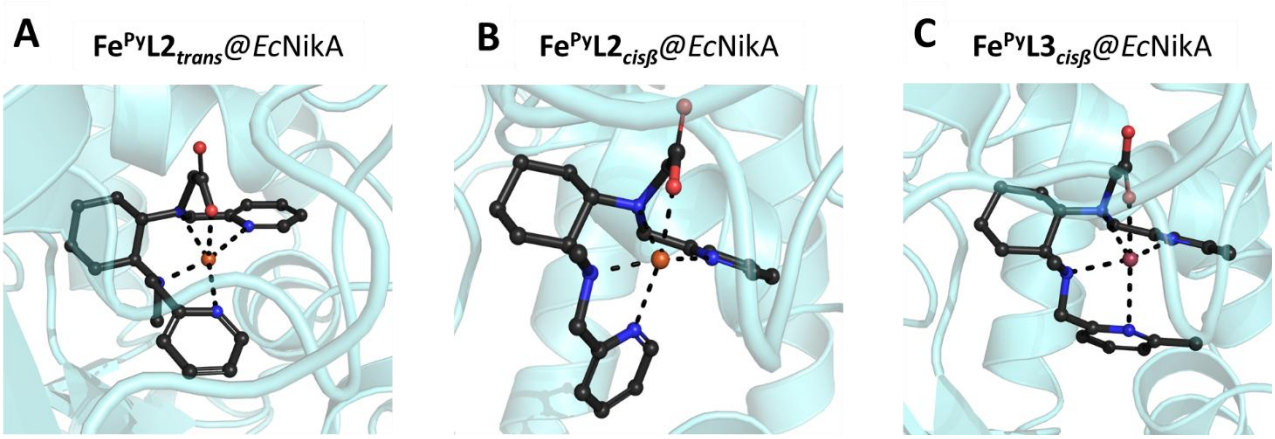

Figure 5. A) Fe^{Py}L2 binding site with the ligand in *trans* topology. The Fe atom is depicted as a red sphere; ^{Py}L2 is illustrated in gray (PDB code: 4DCY, molecule A). B) Fe^{Py}L2 binding site with the ligand in *cisß* topology. The Fe atom is depicted as a red sphere; ^{Py}L2 is illustrated in gray (PDB code: 4DCY, molecule B). C) Fe^{Py}L3 binding site with the ligand in *cisß* topology. The Fe atom is depicted as a red sphere; ^{Py}L3 is illustrated in gray (PDB code: 7A0C).

Interestingly, protein crystallography can also be used as an alternative means to solve the structure of inorganic complexes. Indeed, the structure of Fe(HBED) (see Chart 1)[27] was determined after an oxidation reaction in solution involving the **Fe^{Ph}L0** complex inserted into *Ec*NikA and characterized by X-ray diffraction.[28]

Another great advantage of protein crystals is linked to their high solvent content. For example, orthorhombic *Ec*NikA crystals contain about 51% solvent, thus preserving the enzyme's integrity and activity, but also affording a degree of mobility inside the protein. This mobility contradicts the idea that a crystal is a compact and rigid material. The presence of solvent channels also allows the diffusion of substrates and products to/from the active site. Consequently, reaction mechanisms can be studied by time-dependent trapping of intermediates after adding reactants. This greatly increases the chances of observing key intermediates, compared with attempts to independently crystallize each reaction intermediate. The benefits of protein X-ray crystallography have been fully demonstrated in the field of structural enzymology, with the elucidation of numerous catalytic cycles. In our studies, we have successfully developed this methodology, as shown below. The plasticity of the *Ec*NikA cavity is compatible with stabilization of many ligands, and this versatility is a real asset for the design of ArMs.

2. Various aspects of oxidation catalysis from structure/function studies.

The aim of the *Ec*NikA project was to design oxygenase-mimics through a bioinspired approach, principally by insertion of an inorganic complex into the *Ec*NikA cavity. Our approach was mainly based on inorganic chemistry. Consequently, the metal center was our prime interest in the development of ArMs. Our choices were also dictated by the nature of complexes known to perform selective and enantioselective oxidation catalysis in organic solvents. Initially, we selected iron derivatives with BPMEN, TMC, TPA or HBED-like ligands, the activity of which was nicely demonstrated by the L. Que group in the 1990s. We initially studied these constructs in our laboratory, and our interests later extended to published catalytic systems with different metals.[29] The ligands of these complexes were modified by introducing at least one carboxylate arm, to produce ^{py}**LX,** ^{Ph}**LX** and ^{SC}**LX,** to ensure supramolecular interactions with the *Ec*NikA Arg137 residue (Chart 1). In most cases, as already observed for the TACN, TPA or BPMEN families of iron catalysts, this modification led to a drastic drop in catalytic efficiency, due to the reduced electrophilicity of the oxidative high-valent iron oxo species.[26,30] However, the activity of these complexes was restored following their insertion into *Ec*NikA. This result was a significant contribution to the field. The reasons behind this outcome are detailed in the following chapters. The selectivity controls are also revealed and the stability is found to depend on the physical state of the hybrid.

Fe^{Py}L series

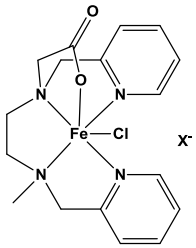

Fe^{Py}L1

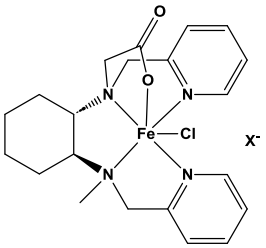

Fe^{Py}L2

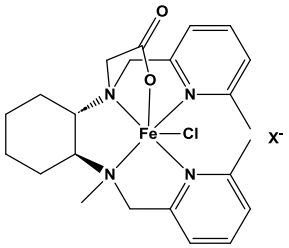

Fe^{Py}L3

Fe^{Ph}L series

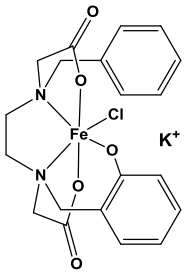

Fe^{Ph}L0

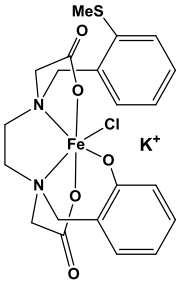

Fe^{Ph}L1

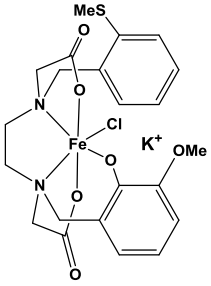

Fe^{Ph}L2

Fe^{Ph}L0 in different oxidation states

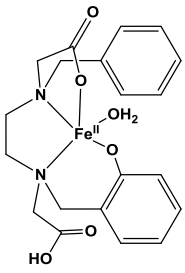

Fe^{Ph}L0$_{red}$

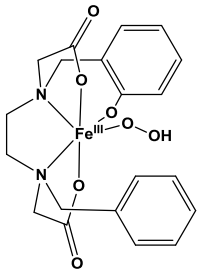

Fe^{Ph}L0$_{int}$

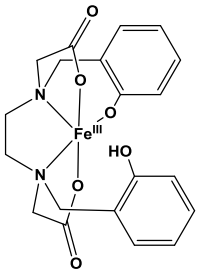

Fe^{Ph}L0$_{ox1}$

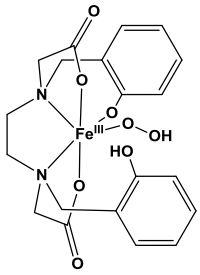

Fe^{Ph}L0$_{int'}$

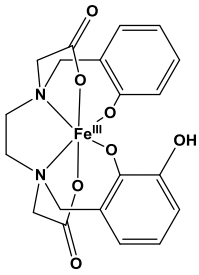

Fe^{Ph}L0$_{ox2}$

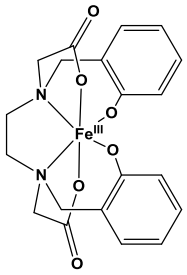

Fe(HBED)

Ru^{Sc}L series

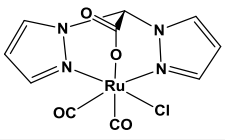

Ru^{Sc}L1

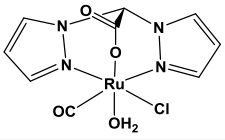

Ru^{Sc}L2

Chart 1. Complexes used in this review.

2.1 Activation of the catalyst

Embedding an inorganic complex into *Ec*NikA in order to design original artificial active sites generally induces modifications to the coordination sites of the complex through two effects: **ligand exchange and/or conformational changes, and alterations to the geometry of the complex**. In our ArMs design strategy, we prioritized the challenging use of complexes that were inactive in aqueous media to allow direct selection of our new hybrid systems based on the generation of a new catalytic activity. Hence, the question arises of how the scaffold affects the stability of the original metal complex. In general, the insertion of Fe and Ru complexes into *Ec*NikA is reported to change the metal coordination sphere. Indeed, the original **Fe^{Ph}LX** complexes contained a chloride as the sixth iron coordination site, as shown by ESI-MS and conductivity experiments in aqueous media.[28] When inserted into the *Ec*NikA cavity, they exchange their chloride ion for a water molecule, as revealed by X-ray crystallography. The same observation was made with the series of **Fe^{Py}LX** complexes.[26] These effects are all linked to our embedding strategy, driven by the presence of a carboxylate in the ligand of the complex which generates a salt bridge with the Arg137. Indeed, chloride ions are known to be labile ligands in the coordination chemistry of iron,[31] and their greater lability here is probably the result of the minor reorganization of the electronic structure of the complex following formation of the salt bridge. Accordingly, a slight shift is observed in the UV-visible spectra of **Fe^{Ph}LX** and **Fe^{Py}LX.** This Cl for H_2O exchange is crucial for activation of the artificial active site; it is reminiscent of the aqua ligand removal observed in the active site of CytP450 during the catalytic cycle of O_2 activation, which was shown to result in a positive shift in the reduction potential of the heme iron atom.[32]

This aspect has been more extensively studied in the case of the **Ru^{Sc}L1**@NikA hybrid, with the release of a strong field ligand.

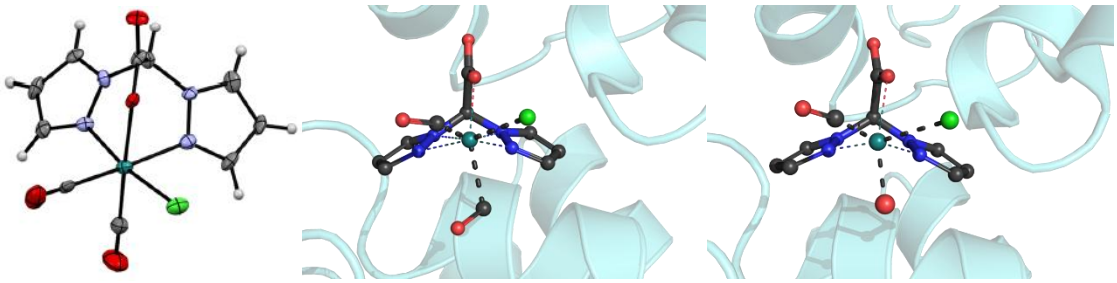

Figure 6. a) Structure of **Ru^{Sc}L1** (CCDC: fsbu18). b) **Ru^{Sc}L1**@NikA (PDB code: 5L8D). c) **Ru^{Sc}L2**@NikA (PDB code: 6R4Q). Ruthenium is depicted as a green sphere, chloride as a light green sphere and water molecules as red spheres. The images were prepared using PyMOL.

The crucial role of the protein environment was highlighted in a study of a hydoxychlorination reaction catalyzed by a **Ru^{Sc}L**@NikA hybrid.[33] As Ru scorpionate complexes were described to perform electrophilic additions in organic solvents, we chose Ru(bpza)$(CO)_2$Cl (**Ru^{Sc}L1**), which mimics the protein environment in the active sites of iron dioxygenases.[29e,34] **Ru^{Sc}L1** was inactive in water. Nevertheless, it converted styrene derivatives into the corresponding hydroxychlorohydrins with very good yields when inserted into the *Ec*NikA protein.[35] The **Ru^{Sc}L1** complex was studied by X-ray diffraction, IR-FT, ESI-MS and conductivity in order to understand the reasons for this huge difference in reactivity. The structure of the complex showed that the ruthenium was surrounded by the bpza ligand, two carbonyl moieties, and a chloride anion (Figure 6a). Conductivity measurements, as well as IR-FT and ESI-MS, showed the loss of the chloride ion in aqueous solution. Conversely, when bound to the protein, whereas the CO and the Cl^- in the equatorial plane are conserved, the coordination sphere of **Ru^{Sc}L1** is modified, with the ligand in the *trans* position to the carboxylate. This could be modelled in different ways depending on the structures analyzed. In some cases, the second CO was observed but with a Ru-CO distance of 2.3 Å (1.9 Å for free **Ru^{Sc}L1**) and a Ru-C-O angle of between 180° and 115°, thus deviating from linearity (Figure 6b). In other structures, a water molecule replaced this CO (Figure 6c), leading to the hypothesis that the second CO ligand was observed just prior to its dissociation. Although the reason for this dissociation remains to be established, it is probably due to the protein binding the ligand's carboxylate *via* a salt bridge (as shown above), to the charge of the protein environment, and to the hydrogen bonding between the CO and two structural water molecules (which are always observed in the cavity). As a consequence, the lability of the CO creates a free position where the oxidant could bind and initiate the oxidation reaction.

Another illustration of the impact of the *Ec*NikA scaffold on complex activation concerns the case of **Fe^{Ph}L0$_{ox1}$** (Figure 7).[28] During the reductive activation of dioxygen by **Fe^{Ph}L0**, the catechol moiety of **Fe^{Ph}L0$_{ox2}$** is produced thanks to two successive hydroxylation processes. The first process generates **Fe^{Ph}L0$_{ox1}$**, and forms a phenol. In the absence of the protein scaffold, the complex tends to reach its thermodynamic state, **Fe(HBED)**, where the resulting phenol has been deprotonated and coordinated to the metal center. As the coordination sphere is completely filled, this complex cannot then undertake the second process. Conversely, the presence of the scaffold stabilizes the uncoordinated phenol moiety, allowing easy reduction of **Fe^{Ph}L0$_{ox1}$**, and triggering the second activation of dioxygen. In this situation, the second coordination sphere avoids coordination between the newly-formed phenol and the metal, affording an appropriate environment for the

protonated state of the phenol moiety and producing the unexpected ligand topology *via* Π stacking interactions (interestingly, the phenol is then sandwiched between the Trp398 and Tyr402, see above on Figure 3B or Figure 4 A-B). Consequently, the **$Fe^{Ph}L0_{ox1}$** complex displays a transient five-coordination site configuration (Figure 6).

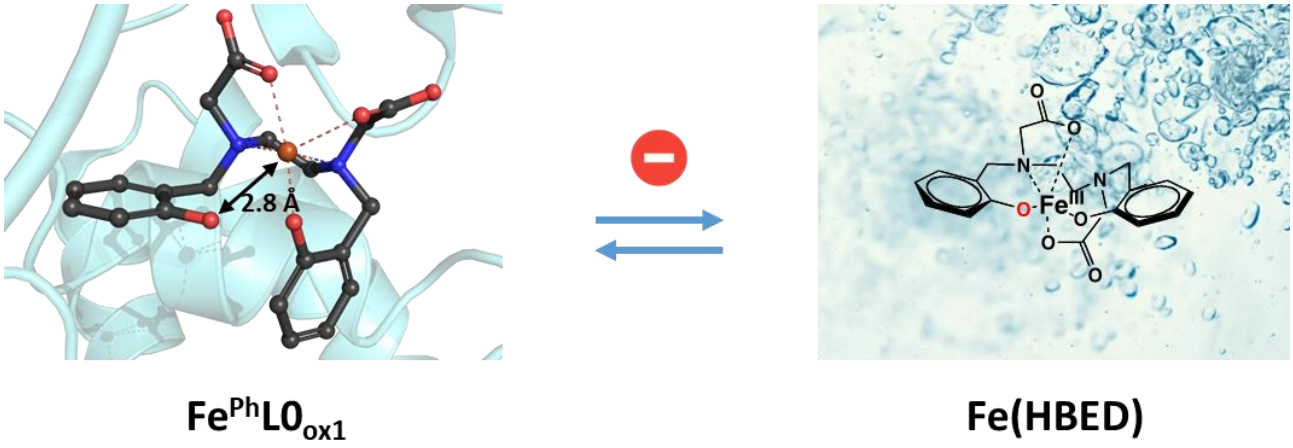

Figure 7. Stabilization of the **$^{Ph}L0_{ox1}$** ligand conformation and coordination modes *via* protein interactions.

To conclude, complexes are activated as a result of their anchoring in the protein cavity, thanks to the creation of labile sites which favor the coordination of the oxidant. These labile sites are regulated by both the conservation of the ligand topology and the modification of the electronic structure of the complexes.

2.2 Reaction selectivity

In addition to being efficient in terms of yield, to be of interest, a reaction must lead to the formation of one or more bonds in a regio-, chemo- and stereoselective way. Several factors may influence the selectivity, and we report here our explanation of this aspect based on the implication of the protein scaffold.

2.2.1 Intrinsic selectivity

The use of *Ec*NikA-based ArMs as catalysts leads to oxidation reactions with perfect chemo- and regio-selectivity. Initially, when we studied sulfoxidation reactions, only sulfoxides were observed, whereas in the absence of the scaffold large amounts of sulfones were detected.[36] Indeed,

molecular docking reveals chemoselectivity to be driven by the cavity's weaker affinity for more polar sulfoxide products than for thioether substrates.

Second, a complete study on chemo-, regio- and stereo-selectivity was conducted when **Ru^{Sc}L1**@NikA (see Chart 1) was used to catalyze the hydroxychlorination of alkenes in a Tris.HCl buffer with diacetoxyiodobenzene (PIDA) as oxidant (Figure 8).[35]

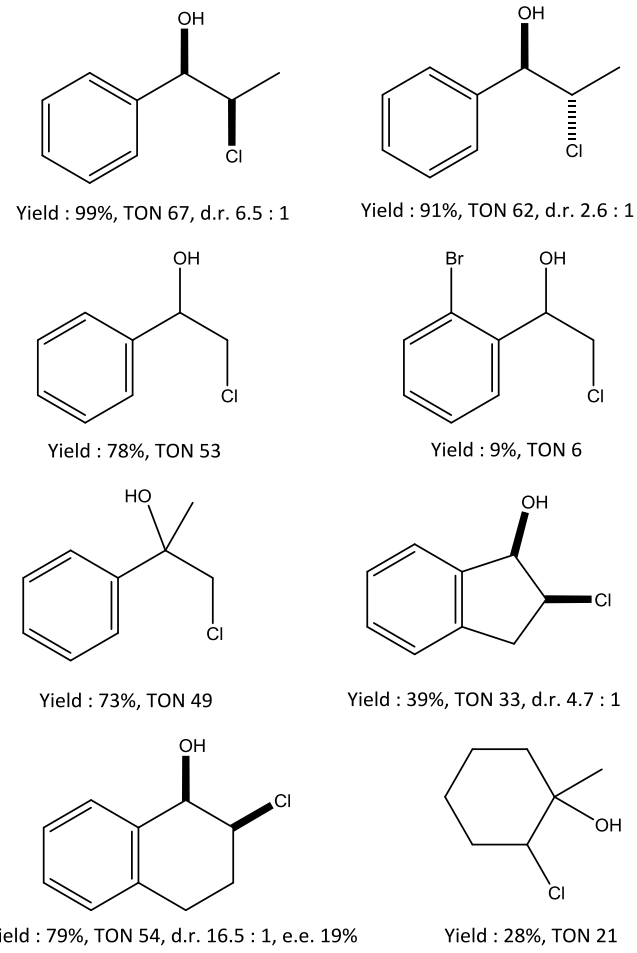

Figure 8. Hydroxychlorination with **Ru1**@NikA in solution. Diastereochemistry indicated corresponding to calculations. Standard conditions: 1/500/600/75 ratio for catalyst/substrate/oxidant/chloride, respectively, for a final **Ru^{Sc}L1** or **Ru^{Sc}L1**@NikA concentration of 37 mM in Tris.HCl (40 mM) pH 7.5 and HEPES (10 mM); reaction at room temperature for 10 min. Yields were calculated relative to initial Cl^- concentration. *e.e*. was calculated from HPLC traces. *d.r*. were calculated from GC traces.

In the case of styrene-derived substrates, yields ranging from 10 to 99% were obtained depending on the nature of the substituent. The presence of an electron-withdrawing bromine substituent gave a very low yield of 10%. However, steric hindrance did not affect the reactivity, since yields of 73 and 79% were obtained for a trisubstituted alkene (α-methylstyrene) and a cyclic alkene (dihydronaphthalene), respectively. When the two diastereoisomers *cis*- and *trans*-β-methylstyrene were used, the exclusive formation of 2-chloro-1-phenylpropanol with yields of over 90% (91% and 99%, respectively) but diastereomeric excesses of 44% and 73%, respectively, were observed. In the case of the cyclic alkene dihydronaphthalene, in addition to a good yield, a very good 90% dia ratio was obtained, along with a weak enantiomeric excess (19%). The catalyst's limits were tested on a non-activated substrate (methylcyclohexene). A moderate yield (28%) was obtained without dia- or enantio-meric excesses, demonstrating that the conjugated aromatic ring has a considerable impact, not only on reactivity, but also on selectivity.

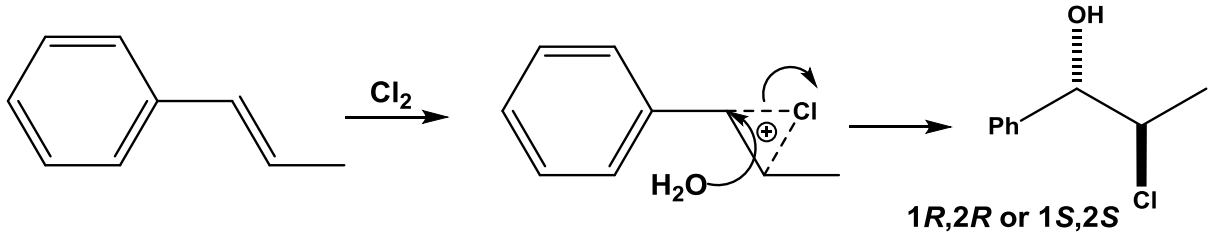

Scheme 1. Expected mechanism for electrophilic addition of chlorine in the presence of water. Only one pair of enantiomers is obtained with a diastereomeric ratio of 100%.

In terms of chemoselectivity, only hydroxychlorohydrins were observed; there were no epoxides or diols. Similarly, complete regioselectivity was observed, leading to the exclusive formation of 2-chloro-1-hydroxy-1-phenyl regioisomers in the case of styrene derivatives. Formation of such a regioisomer suggests that the reaction intermediate is a chloronium ion that reacts with a water molecule on the more electrophilic position stabilized by the phenyl group (Scheme 1). Nevertheless, no Cl_2 formation was detected, and the dia excesses obtained do not support such a mechanism. Moreover, when *p*-methoxystyrene was used under the same reaction conditions, only the epoxide was observed with a 35% yield and complete chemoselectivity.

Could these results be due to the donor nature of the substituent or its para position? Did the protein play a role in selectivity like in previous studies? In an attempt to answer these questions, we turned to theoretical calculations.[33]

Oxidation of *trans*-β-methyl- and 4-methoxy-styrene was studied using computational quantum chemistry with the Gaussian g09 program.[37] The DFT method and B3LYP functional[38] were used with default parameters for most calculations. Due to computational costs, it would have been impossible to examine all of the models encountered in the complete pathways using the full hybrid structure by QM/MM. Accordingly, **Ru^{Sc}L1** and the reactivity of its aqua analog **Ru^{Sc}L2** with PIDA were first investigated by QM; subsequently, the reactivity of both substrates was examined. The influence of the protein on this reactivity was then evaluated by introducing five amino acids close to the ruthenium complex. The results showed that **Ru^{Sc}L1**@NikA was not an active species, and that only **Ru^{Sc}L2**@NikA could react with PIDA to produce a Ru^{IV}(Cl)=O active species. The slightly negative partial charge calculated for the double-bonded oxygen atom in Ru^{IV}(Cl)=O precludes any electrophilic addition on alkenes, leading us to propose a mechanism involving a radical (Scheme 2).

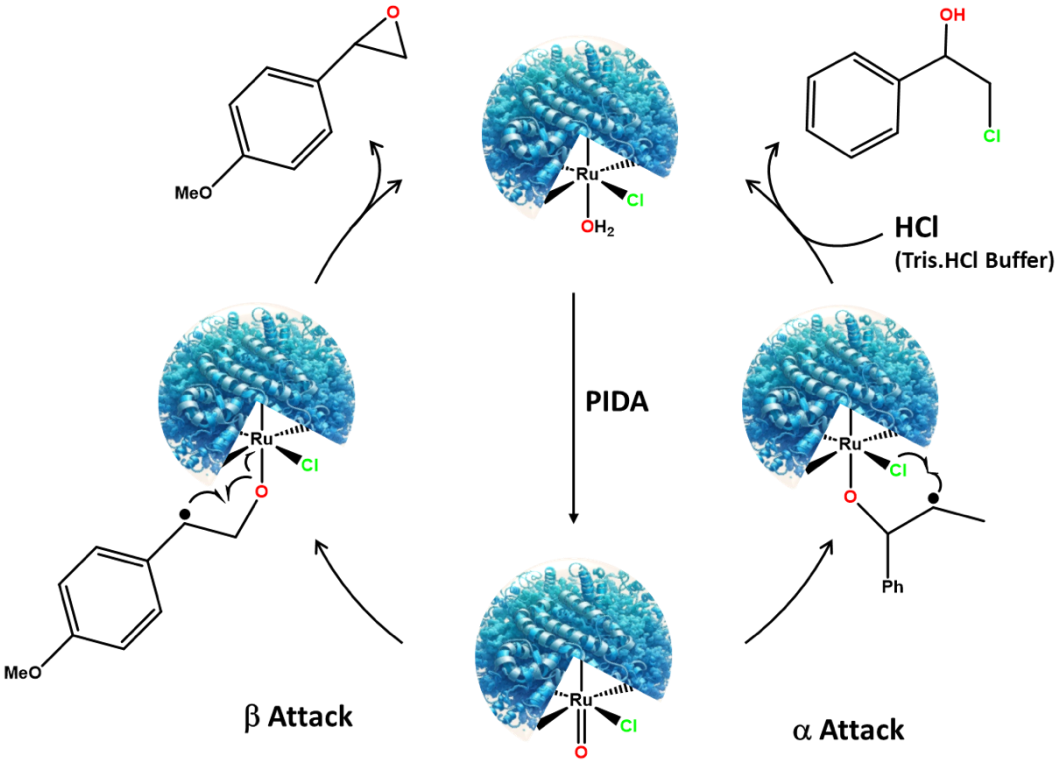

Scheme 2. Proposition of oxidation mechanisms depending on the nature of the substrate.

The radical attack of the Ru^{IV}(Cl)=O on the alkene double bond formed a Ru^{III}-O-C bonded intermediate, which acted like a free radical on the vicinal C atom. This atom could then rotate around the C-C bond before insertion of the chlorine atom or formation of the epoxide ring, in accordance with the variable diastereomeric ratios observed (Figure 9). This intermediate could

also rotate around the C-O bond, influencing chemoselectivity. Indeed, in the case of the non-substituted aromatic ring, the lowest-energy structure presented the radical carbon near the chlorine atom, which reacted rapidly to produce hydroxychlorohydrin. In the presence of the methoxy substituent, this pathway was rejected because of a clash between the surrounding amino acids and the substrate. In this case, the radical carbon was too far from the chlorine, leading it to rearrange to produce the epoxide. This process explains the chemoselectivity. In terms of regioselectivity, as expected, intermediates resulting from the Ru^{IV}(Cl)=O attack on the C2 position led to the lowest energy structures, where the radical carbon atom was stabilized by the phenyl ring. Nevertheless, unlike the kinetic pathway, this thermodynamic pathway did not fit the observed regioselectivity. Indeed, the formation of the chlorohydrin proceeded in a single step with a low barrier of 2.9 kcal/mol and was highly exothermic (ΔE = −33.1 kcal/mol) when Ru^{IV}(Cl)=O attacked on the C1 position.

In summary, the thermodynamics explain the difference in chemoselectivity between the two substrates, the radical nature of the mechanism explains the regioselectivity and the unconcerted mechanism explains the diastereoselectivity. In these reactions, a common intermediate, Ru^{IV}(Cl)=O, emerged from competition between a thermodynamic and a kinetic pathway. The role of the protein environment was highlighted, and it was demonstrated that the selectivity of the artificial enzyme was due to (i) the promotion of the initial oxidizing species through the exchange of a CO ligand, and (ii) how substrate orientation controlled the intermediate structures, formed after the Ru^{IV}(Cl)=O attack: when a C1 attack was preferred, chlorohydrin was formed, whereas attack on C2 produced an epoxide.

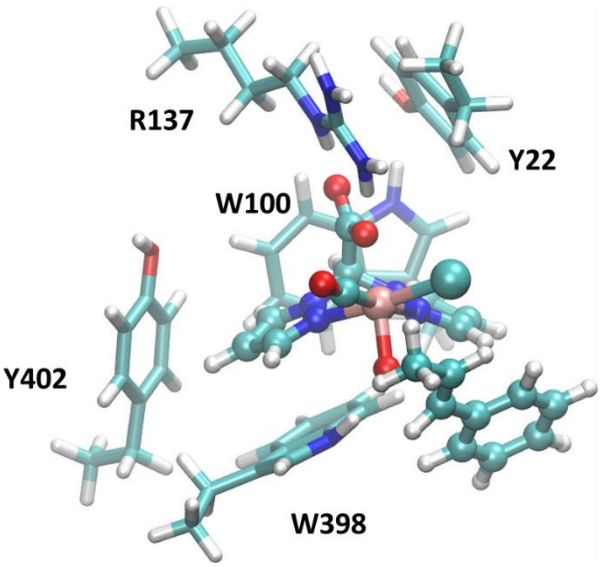

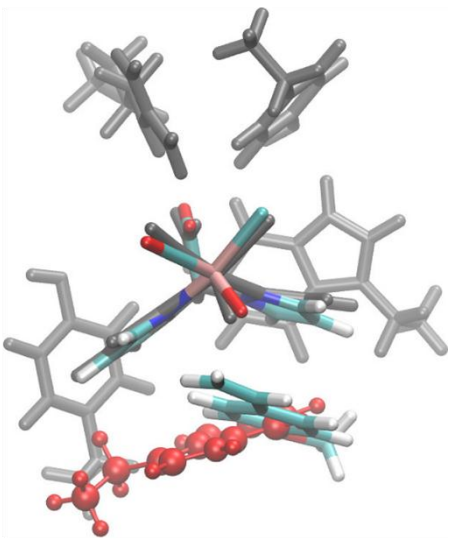

Figure 9. Complexes between Ru(IV)=O and β-methylstyrene (left) or 4-methoxystyrene (right) showing surrounding protein residues. Note the steric clash between 4-methoxystyrene and Trp398 (in red).

2.2.2 Design for selectivity

Whether produced following a structure/reactivity study or serendipitously, enzymes are usually named based on two characteristics: the reaction catalyzed and/or its substrate. These two characteristics have to be taken into account in efforts to design ArMs from scratch. As *Ec*NikA could bind a large panel of metal complexes, we decided to design a sulfoxidase by incorporating an iron complex, **Fe^{Py}L**, known to perform C-H, C=C and C-OH oxidations in organic solvents.[36a] After a simple test on methylphenylsulfide, the best oxidant was selected. To select the right substrate for a putative enzyme, a substrate-binding site had to be modeled for *Ec*NikA. Molecular docking is a powerful method to assess and design protein-ligand interactions between guest catalysts and the surrounding protein environment, particularly when combined with a more precise method (e.g. QM/MM, MD). Docking has been widely used as a second design step to better understand the experimental results of first-generation ArMs and to identify the key residues influencing optimal, directed substrate binding and, consequently, enzymatic activity and substrate selectivity.[39] Here, we add a new string to its bow by searching for the substrate without preconceived ideas.

Molecular docking was thus used to find the potential substrate, based on the X-ray crystallography structure of **Fe^{Py}L1**@NikA. All the molecules containing a C_6H_5-S-CH_2-X motif were extracted from the Zinc database. The Zinc database, with up to 230 million purchasable compounds, was chosen for its ready-to-dock property for virtual screening, which is popular in the pharmaceutical industry.

Several selection criteria based on chemical constraints were added: first, the binding score logP (virtual value for binding energy) for the molecules had to be up to but not greater than 4 to avoid the products becoming blocked in the protein. Second, medium-sized molecules were targeted for synthetic purposes. Third, the main criterion was the Fe…S distance, between the complex and the substrate, determined by the suggested Fe-O…S transition state. Applying these criteria resulted in selection of 374 molecules, in which a family could be identified with a R1-S-CH_2-CONH-R2 motif (*S*- and *N*-substituted thioglycolamide), with aromatic substituents for R1 and R2. The simplest of these molecules was **S0** (2-(3-aminophenyl)sulfanyl-*N*-(1-naphthyl)-acetamide) (R1 = 3-NH_2Ph, R2 = α-naphthyl) (Figure 10). Interestingly, the skeleton of the defined substrate was comparable to that of the major drugs omeprazole and modafinil. **S0** is stabilized in the cavity

of **Fe^{Py}L1**@NikA *via* a hydrogen bond between the aromatic amide function and the Gln385 side chain (Figure 7). An additional interaction was detected with Glu247. A set of molecules derived from **S0** were chosen (**S1**-**S5**), based on the steric hindrance of R1 and R2, and on the absence of the R2 ring. These molecules were used to test how structure differences influence the binding mode. The docking calculations for these molecules indicated that the molecule containing both the R1 and R2 rings was placed in the expected position of **S0**, whereas molecules lacking R2 stabilized at different binding sites, far from the metal center. The concept of virtual selection was validated *via* **S1**-**S6** transformation into sulfoxides. All the molecules superimposed to positions near **S0** were exclusively transformed to their sulfoxide counterparts, whereas molecules lacking R2 were inert under these conditions. Other **Fe^{Py}L** complexes with the particularity of presenting a closed-shell coordination site were inactive under the same catalytic conditions, once again revealing the need for an open shell with a water molecule to trigger activation of the oxidant.

In this work, we implemented an original method to design a selective sulfoxydase, and demonstrated the synergistic effect of each partner. The docking method allowed us to identify a substrate-binding site in the non-enzymatic *Ec*NikA, and to select its appropriate substrate. This is another example of the power of synthetic biology, where a "natural system" is repurposed for broader applications in sustainable chemistry.

Later, the docking-oriented construction of artificial enzymes was validated for all parts of the object.[40] Pordea *et al.*[41] used it for the docking-driven optimization of the supramolecular anchoring of iridium complexes for imine hydrogenation. Docking also performs well in combination with QM/MM methods to define the flexibility of host proteins[42] or to create better enantioselectivity following a Michael addition of nitro alkanes, by identifying the substrate orientations.[43] The concept of *in silico* design has been pushed to its limits for the design of metallohydratases containing a non-natural ligand.[44] Today, the design of new systems benefits considerably from the very dynamic AI revolution.[5a]

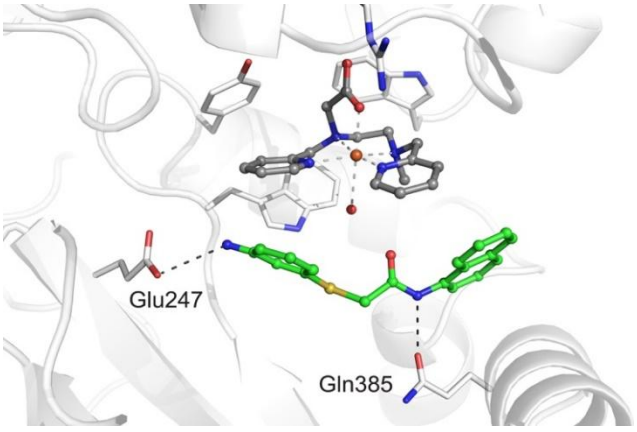

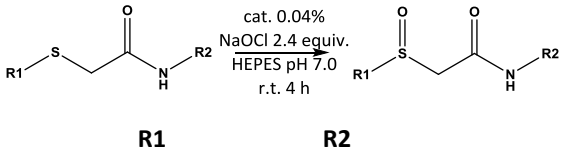

S0	3-NH_2Ph	1-Naphthyl	-
S1	4-$AcNHC_6H_4$	Ph	
S2	4-MeC_6H_4	Ph	
S3	2,5-$(MeO)_2C_6H_3$	Ph	
S4	3,4-$(MeO)_2C_6H_3$	Ph	
S5	2,5-$(MeO)_2C_6H_3$	H	
S6	3,4-$(MeO)_2C_6H_3$	H	

TON: 255-150: , 150-50: , <50: .

Figure 10. Sulfoxidation efficiency with **Fe^{Py}L3**@NikA in solution. The size of the circle is proportional to the selectivity ranging from less than 50% to 100%. Left: **S0** docked to **Fe^{Py}L1**@NikA.

3. *Ec*NikA as a crystal ball

As part of the optimization processes, it is essential to understand reaction mechanisms in chemical catalysis. This implies that each step of the reaction must be determined at a molecular level. To decipher reaction pathways, reaction intermediates need to be trapped and stabilized, or chemical tricks must be used, such as the replacement of substrates by inhibitors, to slow down a reaction process. Protein crystallography has been extensively used in the field of enzymology to characterize intermediates, and unique results have been obtained, notably in the field of O_2 activation by iron enzymes, with revelation of the full catalytic cycle.[45]

This kind of trick was used to decipher O_2 activation by an iron complex, **Fe^{Ph}L0**.[28] This complex has the singularity of containing a phenyl group in its ligand structure, which plays the role of the substrate. This approach is well described in inorganic catalysis, as the proximity between the pseudo substrate and the metal center will mimic the transient substrate:metal complex, to produce a kinetic enhancement.

The insertion of **Fe^{Ph}L0** into **Fe^{III}EDTA**@NikA crystals led the **Fe^{III}EDTA** complex to be replaced by the **Fe^{Ph}L0** complex. The salt bridge between one carboxylate moiety of the **^{Ph}L0** ligand and the Arg137 residue was found to be positioned as expected inside the protein cavity, ensuring the stability of the ferric complex within the protein crystal.

The resulting red crystals were subjected to reductive O_2 activation, corresponding to the activation of the iron by a reductant before the O_2 reacted with the metal center. The complete process caused the color of the protein crystals to change to purple. The X-ray structure of the resulting **Fe^{Ph}L0**@NikA crystals revealed the transformation of the complex **Fe^{Ph}L0** into **Fe^{Ph}L0$_{ox2}$** *via* its double hydroxylation, leading to the generation of a catechol moiety derived from its phenyl group (Figure 11). The full systematic examination of the process by X-ray crystallography demonstrated that the catechol was generated by two successive oxygen transfers from dioxygen. The kinetics of the sequential process was examined, and three reaction intermediates were characterized. First, the reductive step led to the generation of a ferrous state, **Fe^{Ph}L0$_{red}$**, with a

drastic conformational change, provoked by the extra negative charge of the resulting complex. A rearrangement of the metal coordination sphere then allowed the carboxylate moiety to form an additional salt bridge with Arg97 to compensate the overall charge of the system. This led to the positioning of the phenyl ring in a position near the metal center. The second and third intermediates, **Fe^{Ph}L0$_{int}$** and **Fe^{Ph}L0$_{int'}$**, were identified during contact with atmospheric O_2. Both reveal the formation of a peroxo adduct, confirmed by Raman spectroscopy, and differ by the number of hydroxylation steps. The X-ray structure of the peroxo **Fe^{Ph}L0$_{int}$** shows that it points to the phenyl ring, accelerating and driving reaction selectivity. When it was first published, this was the first fully characterized structure of an iron peroxo complex.

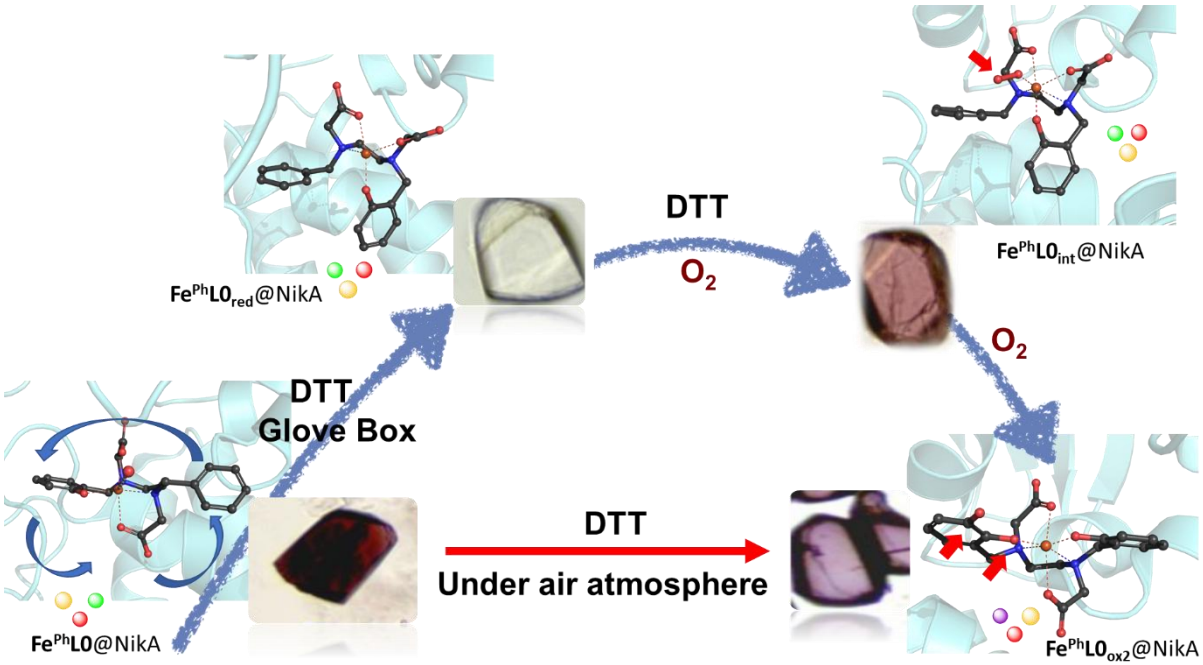

Figure 11. Deciphering a mechanism *via* protein X-ray crystallography. O_2 oxidation reaction of **Fe^{Ph}L0**@NikA *in cristallo*. Red arrows highlight oxidation points. Blue arrows show ligand movements. Signification of colored spheres: yellow: phenol moiety, green: benzyl moiety, red: carboxylate moiety, purple: catechol moiety.

For the selectivity and stability of the complexes described, the role of the protein scaffold is crucial. First, it allows the complex to be trapped in a conformation that the complex alone will not adopt in the ferrous state. Moreover, the intermediate complex, containing one hydroxylation on the phenyl ring (**Fe^{Ph}L0$_{ox1}$**), should not exist in solution (or only very transiently) as the resulting deprotonated ferric complex **Fe(HBED)** is more stable in solution than the free phenol analog. In addition, the orientation of the phenol ring was maintained during the reduction process prior to the second hydroxylation step (see Figure 6).

Moreover, the protein scaffold thus orients the reaction without affecting the electronics of the iron in **Fe^{Ph}L0**. For example, the structure metrics of **Fe(HBED)** were not affected after its insertion into *Ec*NikA. This last point once again highlights the power of this approach and allows us to determine the structure of any iron complex, provided it contains one carboxylate moiety in its ligand. The scaffold is very versatile, allowing the study of the oxidation mechanism without affecting the nature of the observed reactivity but determining the nature of the product.

To conclude, in this section, we presented a new methodology to determine mechanistic pathways, and an alternative to X-ray structure determination for iron-containing inorganic complexes. *Ec*NikA can thus be considered a crystal ball! We could also imagine that these crystals will be able to select complexes. Any such selection should be very efficient, based on the presence of a carboxylate moiety in the ligand. It is also tempting to assume that the charge should discriminate between complexes. As the charge of the cavity is formally +2 (due to the presence of two arginine residues), dianions should be more readily selected than monoanions and cations. This hypothesis is supported by the K_D value as a function of the charge (see above).[9]

In the last decade, Borovik *et al*.[46] developed a method to produce artificial enzymes based on protein-assisted assembly. Using this method, they generated dinuclear iron hydroxo center cores by reengineering the biotin/Sav(streptavidin) technology. Using a similar strategy, the relationship between H bonding and regulation of Cu-hydroperoxide complexes revealed that the stability of the oxidizing species is provided by a single hydrogen bond between the amino acid residue Asp49 and the proximal O-atom of the OO-Cu system.[47]

Another major application of the protein crystal organization consists in its use as a template for nanoparticle synthesis and the design of new biomaterials (drug delivery systems, separation processes).[48] CLEC of cowpea mosaic virus were induced to accumulate Pd^{2+} and Pt^{2+} ions. Under reductive conditions, the resulting metallic nanoparticles aligned in the solvent cavities.[49] Ueno *et al*.[50] used HEWL crystals to embed CoPt nanoparticles. The Pd and Pt ions were bound to distinct sites and their organization in the solvent channels affected the compositions of the CoPt nanoparticles.[50] The same group also functionalized the solvent channels in protein crystals, with very interesting results.[51]

4. Stabilization of ArMs: CLEC *vs in vitro*

Under oxidative conditions, *in vitro* catalysis using *Ec*NikA-based ArMs, although efficient, suffers from a lack of stability compared to when using man-made catalysts. Although in some cases, the

protein scaffold is sufficient to provide a notable stability enhancement for the embedded inorganic complex, in most cases, considerable improvements are needed. A proven chemical approach relies on heterogeneous catalysis, in which the catalyst is grafted onto a solid support. With enzymes, several such strategies have been successful. Covalent binding between a linker on the surface of the support and an amino acid residue using biorthogonal chemistry is quite popular (Michael additions are often favored, the most popular being epoxide for lysine links, or cysteine binding to a maleimide group on the support). A large range of supports from surfaces to MOF and nanoparticles have been developed for immobilization.[15a,52] Another strategy involves encapsulation of the protein in a matrix, *e.g.*, polymers or liposomes, capsids or micelles, or the production of single-enzyme nanoparticles with sizes ranging from nm to µm. One that has particularly attracted our attention is the use of CLEC. Our interest in CLEC is especially motivated by its relevance to our *in cristallo* study (see above).[17a,48,53] This strategy aims to stabilize enzyme crystals by creating covalent bridges using bifunctional molecules, such as dialdehydes, that react with the amino moiety of lysine residues on the surface of neighboring enzyme molecules. This process was originally applied to increase the stability of crystals during X-ray crystallography experiments.[54] This system is well-established for natural enzymes, and there is evidence that the enzyme's activity is conserved or even enhanced *in cristallo*.

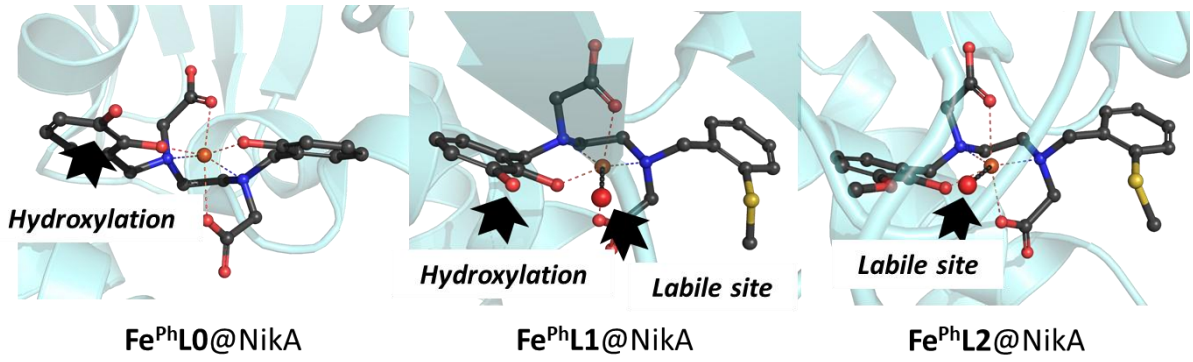

Figure 12. X-ray diffraction studies of hybrids performing an oxidation reaction in the absence of substrate.

The major advantages of the CLEC strategy are: i) high, if not the highest possible, concentration of catalyst in the solid; ii) guaranteed integrity and purity of the enzyme; iii) porosity due to the solvent channels present in the crystals, creating structures akin to mesoporous phases. These solvent channels allow easy diffusion of substrates and products inside the crystalline phase. The CLEC methodology was also adopted by industry (Altus biologics) in the 1990s, thanks to its

excellent operational stability and controllable particle size combined with its easy recovery and reusability. However, at that time, its progression in the market was slowed by the laboriousness and cost of the crystallogenesis step. Examples of CLEC with artificial enzymes are scarce, even if the technique is perfectly fitted for the synthetic methods involved in *de novo* active site reconstitution. This observation has pushed us to develop heterogeneous catalysis by combining *Ec*NikA crystals with inorganic complexes demonstrated as active sites in *in vitro* experiments. The project originated from the observation that **Fe^{Ph}L1**@NikA could react with O_2, but is damaged during catalytic activity by adventitious oxidations of its ligand.[28] Ligand-protecting pathways were therefore sought, the most efficient was identified as the introduction of substitution on the resulting oxidation site (see Chart 1 + Figure 12).

Interestingly, although the substitution on the benzyl ring was intuitive, its impact was quite unexpected. Indeed, the thioether substituent was added to avoid the first step in ligand oxidation, whereas the methoxy substituent was only required because of the prior substitution. In fact, the sulfur atom of the thioether becomes a ligand in the ferrous state, ready for O_2 activation, which prohibits the previous conformational change observed on **Fe^{Ph}L0**@NikA (see above). Consequently, the phenol ring remains in the right position for its attack by the "peroxo intermediate". A methoxy substituent was then added to the phenol ring on **^{Ph}L0** to avoid this over-oxidation. As a result, X-ray crystallography conducted on **Fe^{Ph}L2**@NikA confirmed the absence of ligand oxidation during O_2 activation, opening up the possibility of using exogenous substrates. In addition, from the diverse examples of *in cristallo* oxidation of **Fe^{Ph}L**@NikA, it becomes clear that the oxidizing species points toward the *ortho* position of the aromatic ring, sandwiched between Tyr402 and Trp398, the residues responsible for the selectivity of the O-insertion processes. This fact once again illustrates the importance of the protein scaffold in the catalyst's selectivity.

Table 1. Comparison of oxidative cleavage efficiency of *CLEC***Fe^{Ph}L2**@NikA.

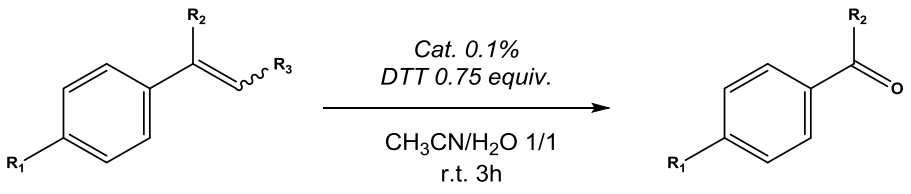

R1	R2	R3	*CLEC*Fe^{Ph}L2@NikA	Fe^{Ph}L2@NikA***	Fe^{Ph}L2	None
H	H	OMe	● *	●	●	●

OMe	H	H	●●**	●	●	●
H	Me	H	●●**	●	●	●
H	H	Ph	●	●	●	●
H	H	*Trans*-Me	●	●	●	●
H	H	*Cis*-Me	●	●	●	●

TON : >500 ●: 250-170 : ●, 100-50 : ●, <50 : ●, 0 : ●.

*Two oxidation products were obtained in a 1:1 ratio. ** After 24 h. ***Catalyses were performed in HEPES buffer 10 mM pH 7.5.

With O_2 as the oxidant, the oxidation of alkenes by *CLEC***Fe^{Ph}L2**@NikA was quite remarkable (Table 1). Thus, *CLEC***Fe^{Ph}L2**@NikA**,** the most stable system, could oxidize *β*-methoxystyrene with O_2 in the presence of excess DTT. Two products were obtained, benzaldehyde and 2-methoxyacetophenone, at yields of 38 and 36%, respectively, and a total TON of 550. In the absence of CLEC, no products were detected, whereas the *in vitro* assay or the **Fe^{Ph}L2** complex alone provided only 23% of the CLEC activity (i.e., a yield of less than 10%). A range of other alkenes could also be transformed into the corresponding benzaldehyde, but with lower yields. Kinetics studies revealed that the reduction step for ferrous formation was the rate-limiting step. Labelling experiments demonstrated that the oxygen atom inserted into the aldehyde was derived from dioxygen, in a non-free-radical process.

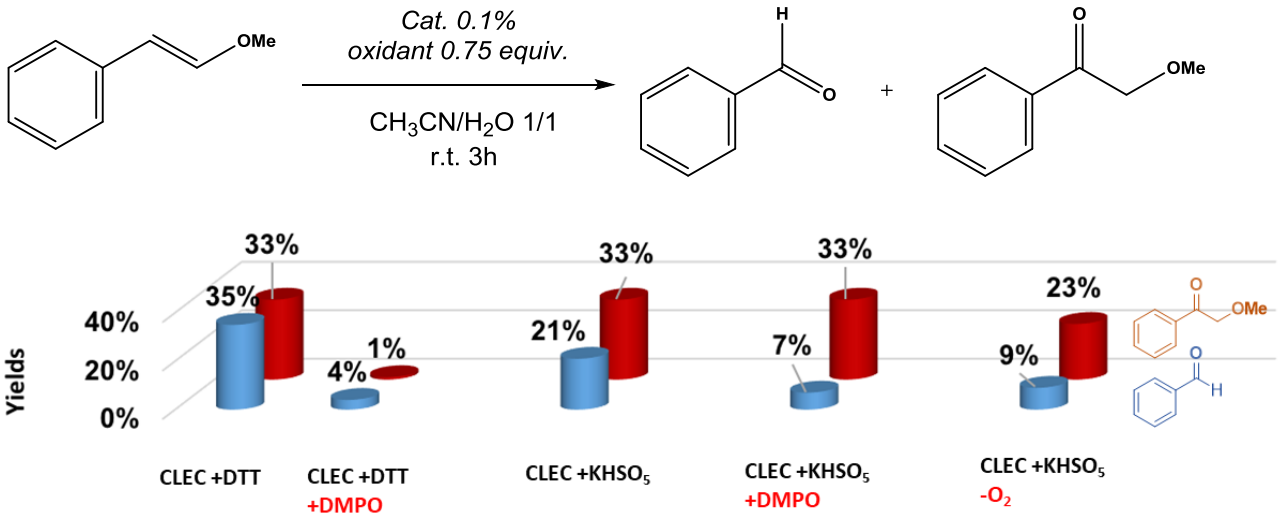

Figure 13. Oxidative cleavage efficiency of *CLEC***Fe^{Ph}L2**@NikA on β-methoxystyrene in various conditions.

To go deeper into the mechanism, a two-electron-oxidant $KHSO_5$ was used and compared to the O_2/DTT system (Figure 13). Both systems showed comparably efficient oxidation of *β*-methoxystyrene, with significantly reduced benzaldehyde yield in the presence of the radical

scavenger DMPO. However, the two systems were distinguished when the presence of DMPO did not affect formation of 2-methoxyacetophenone when using $KHSO_5$. This result suggests that the products are generated through distinct reaction pathways, differing by their radical natures (scheme 3).

A reasonable mechanism is based on the intervention of two distinct metal-based oxidants. First, a superoxo-ferric state initiates the double bond attack. The resulting metal-substrate mono radical O_2 bond system reacts either with O_2, to form the aldehyde *via* C-C breaking, or with DTT, to produce a ketone product *via* a hydroperoxo ferric state. These species were observed by X-ray crystallography during O_2/DTT binding of **Fe^{Ph}L0** (figure 10). The most notable property of CLEC is their stability, with 19 780 turnover numbers during reductive dioxygen activation obtained after 35 recovery steps, attesting to their conserved yield throughout their use. Similar behavior was obtained for $KHSO_5$ during the anti-Markovnikov hydroxychlorination process: after eight recovery steps, 80% of the initial yield was conserved, and only after thirteen recovery steps was the CLEC fully degraded.[55] Conversely, the complex alone or the *in vitro* process were both inactive. Moreover, due to the stability of the CLEC in organic solvents, we were able to extend the reactivity to a wider range of substrates.

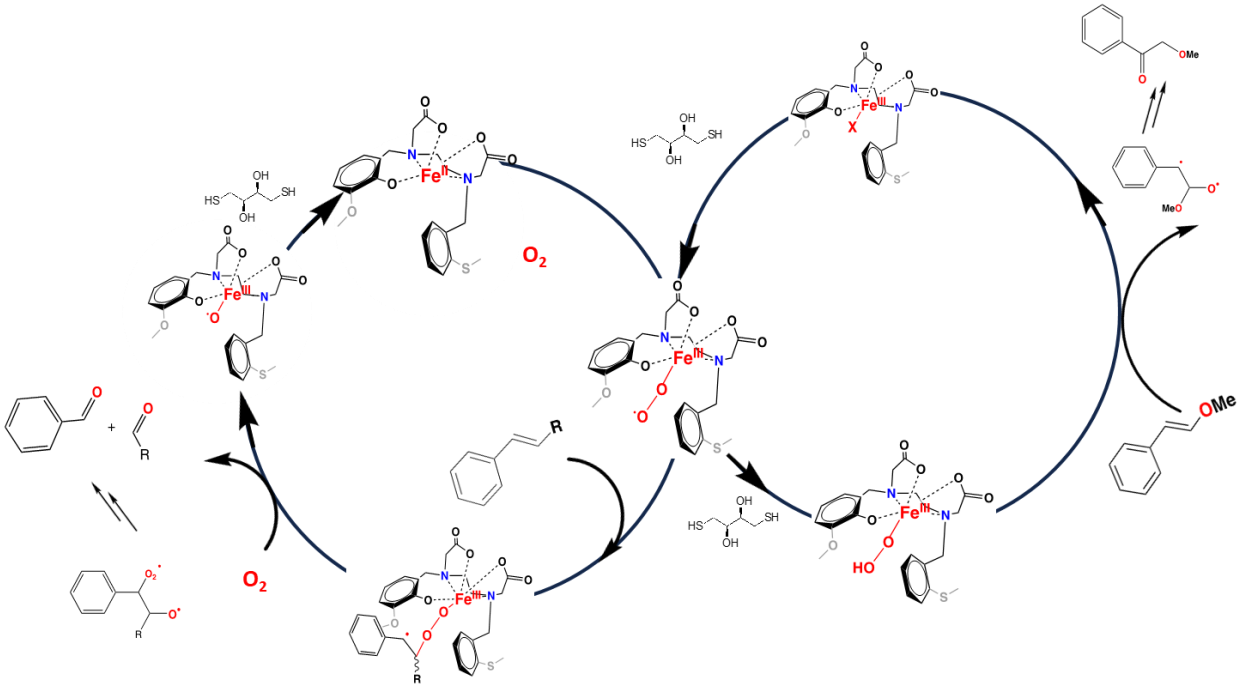

Scheme 3. Proposed oxidation mechanism of styrene derivatives depending on the nature and position of the substituents.

Investigations of another oxidation reaction were also undertaken. Sulfoxidation is quite efficient with *CLEC***Fe^{Py}L5**@NikA on R1-S-CH_2CONH-R2 (N- and S-substituted thioglycolamides), using NaOCl as oxidant, with a high chemoselectivity and fast kinetics (Table 2).[36b] As for the hydroxychlorination reaction, the presence of 50% acetonitrile allows a wider range of substrates to be treated than with buffered solutions.

Several lessons can be drawn from these CLEC studies.

First, the presence of the solid *Ec*NikA causes an **acceleration of the catalytic reactions** that can be attributed to the high density of catalysts inside the porous crystals. This acceleration also obviously correlates with the existence of a substrate-binding site, as already demonstrated by corresponding *in vitro* experiments. The kinetic difference between homogeneous (complex alone) and *in cristallo* conditions may also derive from differences in stability in the organic/aqueous medium. However, if we focus on the active site, a more plausible explanation is that the inorganic complex remains intact in the crystal. In fact, the structure of the inorganic complex is fully conserved in the solid thanks to the crystal's highly ordered arrangement. In contrast, several conformations coexist in solution, and dimeric species cannot be excluded. Finally, the dynamic movements of amino acid residues on the surface of solvent channels could also contribute. To further improve the reaction kinetics, modifications on the solvent channels, as well as on the second coordination sphere of the active site, will be required.

Table 2. Sulfoxidation efficiency with **Fe^{Py}L3**@NikA in solution.

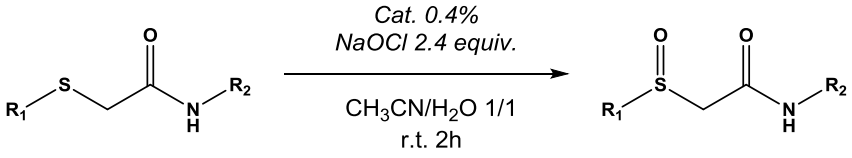

	R1	R2			R1	R2	
S1	4-AcNHC$_6$H$_4$	Ph	● ● *	**S1'**	4-AcNHC$_6$H$_4$	Naphthyl	●
S2	4-MeC$_6$H$_4$	Ph	● ● * ● **	**S2'**	4-MeC$_6$H$_4$	Naphthyl	●
S3	3,4-(MeO)$_2$C$_6$H$_3$	Ph	●	**S3'**	3,4-(MeO)$_2$C$_6$H$_3$	Naphthyl	●
S7	Benzyl	Ph	● ● *	**S7'**	Benzyl	Naphthyl	●

TON: >500 ●, 250-200: ●, 100-50: ●, <50: ●.

The size of the circle is proportional to the yield ranging from less than 15% to 100%. * cat. 0.8% and NaOCl 2.4 equiv..**cat. 0.08% and NaOCl 1 equiv.

Second, the **enhanced stability** derives from the fact that the artificial active site is protected from potential radicals, with the protein playing the role of lightning rod. By ESI-MS, we demonstrated that the protein was oxidized at several positions (10% of the amino acids were modified by an extra oxygen) and partly proteolyzed, at least *in vitro*.[35] The *in cristallo* observation of the conserved integrity under oxidative conditions in all cases appears to confirm that the protein's core is maintained and protected against proteolysis. Overall, it can be suggested that the *in cristallo* arrangement controls substrate/oxidant transfer in the protein, to produce the necessary reactivity and selectivity for full control in the future. Up to now, substrate/oxidant mobility and motion have depended on serendipity.

Third, the CLEC maintain the stability of the complex, making the enzymes compatible with **extreme conditions** such as organic solvent, low pH, and high temperature. In particular, this is demonstrated with $KHSO_5$ in water during hydroxychlorination in the presence of chloride. The oxidizing species is HOCl, formed by the reaction of an iron oxo species – produced by the heterolytic cleavage of a Fe-OO-S(O_2)-OH species by chloride – that delivers H^+ up to pH 2 during the reaction. At this pH, the hybrids precipitate and the complex alone is decomposed. In contrast, the whole catalyst conserves its integrity when in the CLEC form.

Fourth, the use of organic solvents expands the range of soluble substrates relative to *in vitro* catalysis. In summary, the *Ec*NikA crystals favor **compartmentalization**, selecting one major reactive pathway by strictly controlling the environment surrounding the catalytic complex. They also help to enhance complex stability in extreme conditions. Finally, the **packing** within the crystals controls the reaction rate.

One aspect remains unexplained: the **activity switch**, if we omit ligand exchange (see above). The *in vitro vs in cristallo* balance is not trivial. The first suggestion is that the hydrophobic nature of the environment is quite different, influencing the reaction conditions. The second suggestion is that the relatively poor protein motility in the solid should slow down the kinetics. Conversely, the kinetics are under the control of the relative concentrations of each reaction partner – both high in the crystal. Indeed, the crystal may play the role of a funnel.

As stated before, there are few examples in the literature of CLEC versions of artificial enzymes performing oxidation catalysis. Ueno *et al*.[56] designed the insertion in engineered porous lysozyme crystals to perform the enantioselective reduction of ketones by a Ru arene complex, achieving up to 36% enantiomeric excess. Here, the complex was found to be stabilized in the protein *via* an

imidazole from a histidine binding to the metal. More recently, hydrogenase mimics were designed on the same construction drawings.[57]

The future of ArMs CLECs in applications such as industrial catalysts is still under debate. The challenge of crystallogenesis is partly behind us thanks to technological progress in protein crystallization and the use of robotics to facilitate production of solid biohybrids. However, the cost of crystallogenesis, although dropping, remains a drawback for this strategy. Moreover, the future of ArMs CLECs depends on the original reaction catalyzed. If no *in vitro* alternative is found, the crystallization approach becomes crucial. The future of these constructs also depends on their use in the field of catalysis for energy. In this case, the substrate is often a gas, CO_2 or H_2. this property should make the mesoporous nature of the protein crystals a great asset, since many examples derived from O_2 reaction exist. Finally, their use as a support in electrocatalysis may open up exciting future opportunities, such as following the deposition of crystals on electron-active materials.

CONCLUSION

The field of artificial enzymes is growing rapidly thanks to the contributions of synthetic biology as a tool for sustainable chemistry. As the design concepts are now well mastered, the field is shifting to the search for abiotic transformations at the level of the efficiency of natural enzymes, in terms of kinetics and selectivity. Moreover, ArMs are also expected to be useful in complex transformations, with contributions from compartmentalization concepts associated with reaction cascades. In terms of the contribution of *Ec*NikA, we have highlighted the unique properties that it confers on bioinspired catalysts, at the intersection between biochemistry and chemistry, for the creation of alternatives to natural enzymes. We have demonstrated a means to enhance selectivity and stability, in particular by switching from *in vitro* to *in cristallo* conditions. *In cristallo* catalysis is absolutely fascinating, because it easily combines studies of reaction mechanisms and of catalysis, while also providing *in operando* conditions. Even if its use in biotechnological processes remains far off for large-scale production, it appears feasible to use it today in small-scale applications based on microfluidics.

The ArMs derived from the active reconstitution strategy represent a nice playground for inorganic chemists, leaving them free to test chemical rationales derived from inorganic chemistry principles. The first challenge in the design of ArMs is to choose the right enzyme capable of

binding our systems. The *Ec*NikA system is interesting as it has a versatile ability to bind a large panel of complexes, making it possible to develop any kind of reaction. The *in cristallo* version is promising in terms of efficiency and stability. Nevertheless, one aspect that needs to be more carefully scrutinized is the enantioselectivity, potentially modifiable *via* mutagenesis studies, providing the resulting structures are compatible with cristallogenesis. In our collaborative projects, a few *Ec*NikA mutants have been designed, most of which can be crystalized. We recently managed to run epoxidation reactions, with moderate yields but with a high ee (up to 90%). These results reveal that transformation of the *Ec*NikA cavity should provide enantioselectivity. Finally, to ensure their usefulness in industry, the *in vivo* conditions must be mastered to meet synthetic biology needs. Even though the number of successes reported so far is small, the production of artificial enzymes is still in its infancy, and real technological challenges have yet to be overcome. The next step, which we have started, will therefore be to transfer the *Ec*NikA technology to *in vivo* studies.

To conclude, this *Ec*NikA adventure as a whole depended on the eye and on the expectations of inorganic chemists, based on bioinspired catalysis concepts. For one of us, the motivation for bioinspired chemistry is partly linked to the chance to rub shoulders with Prof Lawrence Que Jr. and to learn from his major contributions to bioinorganic chemistry. Scientific discussions have always been a source of inspiration, as he always says: “chemistry is telling us something” and it will continue to do so.

Table of abbreviations

ArMs	Artificial metalloenzymes	HBED	N,N’-Di(2-hydroxybenzyl)ethylenediamine-N,N’-diacetic acid
CLEC	Cross-linked enzyme crystals	BPMEN	N,N’-Bipyridyl-N,N’-dimethylethylenediamine
TMDs	Transmembrane proteins	TMC	1,4,8,11-tetraaza-1,4,8,11-tetramethylcyclotetradecane
NBD	Nucleotide-binding protein	TPA	Tris(2-pyridylmethyl)amine
SBP	Soluble binding protein	TACN	Triazacyclononane
Ni-BP	Nickel binding protein	HBpza	bis(pyrazol-1-yl)acetate
EDTA	Ethylenediaminetatraacetic acid	PIDA	Phenyliodine diacetate

REFERENCES

(1) a) Hirschi, S.; Ward, T. R.; Meier, W. P.; Müller, D. J.; Fotiadis, D. "Synthetic Biology: Bottom-Up Assembly of Molecular Systems" *Chem. Rev.* **2022**, *122*, 16294; b) Chen, X.; Gao, C.; Guo, L.; Hu, G.; Luo, Q.; Liu, J.; Nielsen, J.; Chen, J.; Liu, L. "DCEO Biotechnology: Tools To Design, Construct, Evaluate, and Optimize the Metabolic Pathway for Biosynthesis of Chemicals" *Chem. Rev.* **2018**, *118*, 4.

(2) a) Arnold, F. H. "Innovation by Evolution: Bringing New Chemistry to Life (Nobel Lecture)" *Angew. Chem. Int. Ed.* **2019**, *58*, 14420; b) Davis, H. J.; Ward, T. R. "Artificial Metalloenzymes: Challenges and Opportunities" *ACS Central Science* **2019**, *5*, 1120.

(3) Dydio, P.; Key, H. M.; Nazarenko, A.; Rha, J. Y.-E.; Seyedkazemi, V.; Clark, D. S.; Hartwig, J. F. "An artificial metalloenzyme with the kinetics of native enzymes" *Science* **2016**, *354*, 102.

(4) Hammer, S. C.; Kubik, G.; Watkins, E.; Huang, S.; Minges, H.; Arnold, F. H. "Anti-Markovnikov alkene oxidation by metal-oxo–mediated enzyme catalysis" *Science* **2017**, *358*, 215.

(5) a) Kalvet, I.; Ortmayer, M.; Zhao, J.; Crawshaw, R.; Ennist, N. M.; Levy, C.; Roy, A.; Green, A. P.; Baker, D. "Design of Heme Enzymes with a Tunable Substrate Binding Pocket Adjacent to an Open Metal Coordination Site" *J. Am. Chem. Soc.* **2023**, *145*, 14307; b) Eisenstein, M. "AI-enhanced protein design makes proteins that have never existed" *Nat. Biotechnol.* **2023**, *41*, 303.

(6) Mukherjee, G.; Satpathy, J. K.; Bagha, U. K.; Mubarak, M. Q. E.; Sastri, C. V.; de Visser, S. P. "Inspiration from Nature: Influence of Engineered Ligand Scaffolds and Auxiliary Factors on the Reactivity of Biomimetic Oxidants" *ACS Catal.* **2021**, *11*, 9761.

(7) a) Van Stappen, C.; Deng, Y.; Liu, Y.; Heidari, H.; Wang, J.-X.; Zhou, Y.; Ledray, A. P.; Lu, Y. "Designing Artificial Metalloenzymes by Tuning of the Environment beyond the Primary Coordination Sphere" *Chem. Rev.* **2022**, *122*, 11974; b) Yu, F.; Cangelosi, V. M.; Zastrow, M. L.; Tegoni, M.; Plegaria, J. S.; Tebo, A. G.; Mocny, C. S.; Ruckthong, L.; Qayyum, H.; Pecoraro, V. L. "Protein Design: Toward Functional Metalloenzymes" *Chem. Rev.* **2014**, *114*, 3495; c) Koebke, K. J.; Pinter, T. B. J.; Pitts, W. C.; Pecoraro, V. L. "Catalysis and Electron Transfer in De Novo Designed Metalloproteins" *Chem. Rev.* **2022**, *122*, 12046; d) Schwizer, F.; Okamoto, Y.; Heinisch, T.; Gu, Y.; Pellizzoni, M. M.; Lebrun, V.; Reuter, R.; Köhler, V.; Lewis, J. C.; Ward, T. R. "Artificial Metalloenzymes: Reaction Scope and Optimization Strategies" *Chem. Rev.* **2018**, *118*, 142; e) Marchi-Delapierre, C.; Rondot, L.; Cavazza, C.; Ménage, S. "Oxidation Catalysis by Rationally Designed Artificial Metalloenzymes" *Isr. J. Chem.* **2015**, *55*, 61.

(8) a) Lu, Y.; Yeung, N.; Sieracki, N.; Marshall, N. M. "Design of functional metalloproteins" *Nature* **2009**, *460*, 855; b) Mirts, E. N.; Petrik, I. D.; Hosseinzadeh, P.; Nilges, M. J.; Lu, Y. "A designed heme-[4Fe-4S] metalloenzyme catalyzes sulfite reduction like the native enzyme" *Science* **2018**, *361*, 1098.

(9) Cherrier, M. V.; Girgenti, E.; Amara, P.; Iannello, M.; Marchi-Delapierre, C.; Fontecilla-Camps, J. C.; Menage, S.; Cavazza, C. "The structure of the periplasmic nickel-binding protein NikA provides insights for artificial metalloenzyme design" *J. Biol. Inorg. Chem.* **2012**, *17*, 817.

(10) a) Kawakami, N.; Shoji, O.; Watanabe, Y. "Use of Perfluorocarboxylic Acids To Trick Cytochrome P450BM3 into Initiating the Hydroxylation of Gaseous Alkanes" *Angew. Chem. Int. Ed.* **2011**, *50*, 5315; b) Zilly, F. E.; Acevedo, J. P.; Augustyniak, W.; Deege, A.; Häusig, U. W.; Reetz, M. T. "Tuning a P450 Enzyme for Methane Oxidation" *Angew. Chem. Int. Ed.* **2011**, *50*, 2720; c) Yonemura, K.; Ariyasu, S.; Stanfield, J. K.; Suzuki, K.; Onoda, H.; Kasai, C.; Sugimoto, H.; Aiba, Y.; Watanabe, Y.; Shoji, O. "Systematic Evolution of Decoy Molecules for the Highly Efficient

Hydroxylation of Benzene and Small Alkanes Catalyzed by Wild-Type Cytochrome P450BM3" *ACS Catal.* **2020**, *10*, 9136.
(11) a) Oohora, K.; Onoda, A.; Hayashi, T. "Hemoproteins Reconstituted with Artificial Metal Complexes as Biohybrid Catalysts" *Acc. Chem. Res.* **2019**, *52*, 945; b) Ueno, T.; Abe, S.; Yokoi, N.; Watanabe, Y. "Coordination design of artificial metalloproteins utilizing protein vacant space" *Coord. Chem. Rev.* **2007**, *251*, 2717; c) Mahy, J.-P.; Maréchal, J.-D.; Ricoux, R. "Various strategies for obtaining oxidative artificial hemoproteins with a catalytic oxidative activity: from "Hemoabzymes" to "Hemozymes"?" *J. Porphyr. Phthalocyanines* **2014**, *18*, 1063.
(12) Liang, A. D.; Serrano-Plana, J.; Peterson, R. L.; Ward, T. R. "Artificial Metalloenzymes Based on the Biotin–Streptavidin Technology: Enzymatic Cascades and Directed Evolution" *Acc. Chem. Res.* **2019**, *52*, 585.
(13) a) Oelerich, J.; Roelfes, G. "DNA-based asymmetric organometallic catalysis in water" *Chem. Sci.* **2013**, *4*, 2013; b) Kariyawasam, K.; Di Meo, T.; Hammerer, F.; Valerio-Lepiniec, M.; Sciortino, G.; Maréchal, J.-D.; Minard, P.; Mahy, J.-P.; Urvoas, A.; Ricoux, R. "An Artificial Hemoprotein with Inducible Peroxidase- and Monooxygenase-Like Activities" *Chem. Eur. J.* **2020**, *26*, 14929; c) Serrano-Plana, J.; Rumo, C.; Rebelein, J. G.; Peterson, R. L.; Barnet, M.; Ward, T. R. "Enantioselective Hydroxylation of Benzylic C(sp3)–H Bonds by an Artificial Iron Hydroxylase Based on the Biotin–Streptavidin Technology" *J. Am. Chem. Soc.* **2020**, *142*, 10617.
(14) Drienovská, I.; Rioz-Martínez, A.; Draksharapu, A.; Roelfes, G. "Novel artificial metalloenzymes by in vivo incorporation of metal-binding unnatural amino acids" *Chem. Sci.* **2015**, *6*, 770.
(15) a) Chapman, R.; Stenzel, M. H. "All Wrapped up: Stabilization of Enzymes within Single Enzyme Nanoparticles" *J. Am. Chem. Soc.* **2019**, *141*, 2754; b) Wang, K.-Y.; Zhang, J.; Hsu, Y.-C.; Lin, H.; Han, Z.; Pang, J.; Yang, Z.; Liang, R.-R.; Shi, W.; Zhou, H.-C. "Bioinspired Framework Catalysts: From Enzyme Immobilization to Biomimetic Catalysis" *Chem. Rev.* **2023**, *123*, 5347; c) Küchler, A.; Yoshimoto, M.; Luginbühl, S.; Mavelli, F.; Walde, P. "Enzymatic reactions in confined environments" *Nat. Nanotech.* **2016**, *11*, 409; d) Chen, W.-H.; Vázquez-González, M.; Zoabi, A.; Abu-Reziq, R.; Willner, I. "Biocatalytic cascades driven by enzymes encapsulated in metal–organic framework nanoparticles" *Nature Catalysis* **2018**, *1*, 689.
(16) Sheldon, R. A.; van Pelt, S. "Enzyme immobilisation in biocatalysis: why, what and how" *Chem. Soc. Rev.* **2013**, *42*, 6223.
(17) a) Margolin, A. L.; Navia, M. A. "Protein crystals as novel catalytic materials" *Angew. Chem. Int. Ed.* **2001**, *40*, 2204; b) Roy, J. J.; Abraham, E. T. "Strategies in making cross-linked enzyme crystals" *Chem. Rev.* **2004**, *104*, 3705; c) Quiocho, F. A.; Richards, F. M. "Intermolecular Cross Linking of a Protein in the Crystalline State : Carbopeptidase-A" *PNAS* **1964**, *52*, 833; d) Persichetti, R. A.; Clair, N. L. S.; Griffith, J. P.; Navia, M. A.; Margolin, A. L. "Cross-Linked Enzyme Crystals (CLECs) of Thermolysin in the Synthesis of Peptides" *J. Am. Chem. Soc.* **1995**, *117*, 2732.
(18) Chivers, P. T. "Nickel recognition by bacterial importer proteins" *Metallomics* **2015**, *7*, 590.
(19) Cui, J.; Davidson, A. L. "ABC solute importers in bacteria" *Essays Biochem.* **2011**, *50*, 85.
(20) Wu, L. F.; Mandrand-Berthelot, M. A.; Waugh, R.; Edmonds, C. J.; Holt, S. E.; Boxer, D. H. "Nickel deficiency gives rise to the defective hydrogenase phenotype of hydC and fnr mutants in Escherichia coli" *Mol. Microbiol.* **1989**, *3*, 1709.
(21) Mao, B.; McCammon, J. A. "Structural study of hinge bending in L-arabinose-binding protein" *J. Biol. Chem.* **1984**, *259*, 4964.
(22) Heddle, J.; Scott, D. J.; Unzai, S.; Park, S.-Y.; Tame, J. R. H. "Crystal Structures of the Liganded and Unliganded Nickel-binding Protein NikA from Escherichia coli" *J. Biol. Chem.* **2003**, *278*, 50322.

(23) Cherrier, M. V.; Martin, L.; Cavazza, C.; Jacquamet, L.; Lemaire, D.; Gaillard, J.; Fontecilla-Camps, J. C. "Crystallographic and spectroscopic evidence for high affinity binding of FeEDTA(H2O)(-) to the periplasmic nickel transporter NikA" *J. Am. Chem. Soc.* **2005**, *127*, 10075.
(24) Chivers, P. T.; Benanti, E. L.; Heil-Chapdelaine, V.; Iwig, J. S.; Rowe, J. L. "Identification of Ni-(L-His)$_2$ as a substrate for NikABCDE-dependent nickel uptake in Escherichia coli" *Metallomics* **2012**, *4*, 1043.
(25) Lebrette, H.; Iannello, M.; Fontecilla-Camps, J. C.; Cavazza, C. "The binding mode of Ni-(L-His)2 in NikA revealed by X-ray crystallography" *J. Inorg. Biochem.* **2013**, *121*, 16.
(26) Oddon, F.; Girgenti, E.; Lebrun, C.; Marchi-Delapierre, C.; Pécaut, J.; Ménage, S. "Iron Coordination Chemistry of N2Py2 Ligands Substituted by Carboxylic Moieties and Their Impact on Alkene Oxidation Catalysis" *Eur. J. Inorg. Chem.* **2012**, *2012*, 85.
(27) Motekaitis, R. J.; Martell, A. E.; Welch, M. J. "Stabilities of trivalent metal complexes of phenolic ligands related to N,N'-bis(2-hydroxybenzyl)ethylenediamine-N,N'-diacetic acid (HBED)" *Inorg. Chem.* **1990**, *29*, 1463.
(28) Cavazza, C.; Bochot, C.; Rousselot-Pailley, P.; Carpentier, P.; Cherrier, M. V.; Martin, L.; Marchi-Delapierre, C.; Fontecilla-Camps, J. C.; Menage, S. "Crystallographic snapshots of the reaction of aromatic C-H with O-2 catalysed by a protein-bound iron complex" *Nat. Chem.* **2010**, *2*, 1069.
(29) a) Que, L.; Tolman, W. B. "Biologically inspired oxidation catalysis" *Nature* **2008**, *455*, 333; b) Costas, M.; Mehn, M. P.; Jensen, M. P.; Que, L. "Dioxygen activation at mononuclear nonheme iron active sites: Enzymes, models, and intermediates" *Chem. Rev.* **2004**, *104*, 939; c) Chen, K.; Que, L. "Stereospecific alkane hydroxylation by non-heme iron catalysts: Mechanistic evidence for an Fe-V = O active species" *J. Am. Chem. Soc.* **2001**, *123*, 6327; d) McDonald, A. R.; Que, L. "High-valent nonheme iron-oxo complexes: Synthesis, structure, and spectroscopy" *Coord. Chem. Rev.* **2013**, *257*, 414; e) Tuerkoglu, G.; Tampier, S.; Strinitz, F.; Heinemann, F. W.; Huebner, E.; Burzlaff, N. "Ruthenium Carbonyl Complexes Bearing Bis(pyrazol-1-yl)carboxylato Ligands" *Organometallics* **2012**, *31*, 2166; f) Sastri, C. V.; Lee, J.; Oh, K.; Lee, Y. J.; Lee, J.; Jackson, T. A.; Ray, K.; Hirao, H.; Shin, W.; Halfen, J. A.; Kim, J.; Que, L.; Shaik, S.; Nam, W. "Axial ligand tuning of a nonheme iron(IV)–oxo unit for hydrogen atom abstraction" *PNAS* **2007**, *104*, 19181.
(30) a) Costas, M.; Chen, K.; Que, L. "Biomimetic nonheme iron catalysts for alkane hydroxylation" *Coord. Chem. Rev.* **2000**, *200*, 517; b) Bigelow, J. O.; England, J.; Klein, J. E. M. N.; Farquhar, E. R.; Frisch, J. R.; Martinho, M.; Mandal, D.; Münck, E.; Shaik, S.; Que, L., Jr. "Oxoiron(IV) Tetramethylcyclam Complexes with Axial Carboxylate Ligands: Effect of Tethering the Carboxylate on Reactivity" *Inorg. Chem.* **2017**, *56*, 3287.
(31) Mekmouche, Y.; Ménage, S.; Pécaut, J.; Lebrun, C.; Reilly, L.; Schuenemann, V.; Trautwein, A.; Fontecave, M. "Mechanistic Tuning of Hydrocarbon Oxidations with H2O2, Catalyzed by Hexacoordinate Ferrous Complexes" *Eur. J. Inorg. Chem.* **2004**, *2004*, 3163.
(32) Daff, S. N.; Chapman, S. K.; Holt, R. A.; Govindaraj, S.; Poulos, T. L.; Munro, A. W. "Redox Control of the Catalytic Cycle of Flavocytochrome P-450 BM3" *Biochemistry* **1997**, *36*, 13816.
(33) Lopez, S.; Mayes, D. M.; Crouzy, S.; Cavazza, C.; Leprêtre, C.; Moreau, Y.; Burzlaff, N.; Marchi-Delapierre, C.; Ménage, S. "A Mechanistic Rationale Approach Revealed the Unexpected Chemoselectivity of an Artificial Ru-Dependent Oxidase: A Dual Experimental/Theoretical Approach" *ACS Catal.* **2020**, *10*, 5631.
(34) Turkoglu, G.; Heinemann, F. W.; Burzlaff, N. "Transition metal complexes bearing a 2,2-bis(3,5-dimethylpyrazol-1-yl)propionate ligand: one methyl more matters" *Dalton Trans.* **2011**, *40*, 4678.

(35) Lopez, S.; Rondot, L.; Cavazza, C.; Iannello, M.; Boeri-Erba, E.; Burzlaff, N.; Strinitz, F.; Jorge-Robin, A.; Marchi-Delapierre, C.; Menage, S. "Efficient conversion of alkenes to chlorohydrins by a Ru-based artificial enzyme" *Chem. Commun.* **2017**, *53*, 3579.
(36) a) Esmieu, C.; Cherrier, M. V.; Amara, P.; Girgenti, E.; Marchi-Delapierre, C.; Oddon, F.; Iannello, M.; Jorge-Robin, A.; Cavazza, C.; Ménage, S. "An artificial oxygenase built from scratch : the importance of the substrate-binding site revealed by a docking approach" *Angew. Chem. Int. Ed.* **2013**, *52*, 3922; b) Lopez, S.; Marchi-Delapierre, C.; Cavazza, C.; Ménage, S. "A Selective Sulfide Oxidation Catalyzed by Heterogeneous Artificial Metalloenzymes Iron@NikA" *Chem. Eur. J.* **2020**, *26*, 16633.
(37) Frisch, M. J.; Trucks, G. W.; Schlegel, H. B.; Scuseria, G. E.; Robb, M. A.; Cheeseman, J. R.; Montgomery, J., J. A.; ; Vreven, T.; Kudin, K. N.; Burant, J. C.; Millam, J. M.; Lyengar, S. S.; Tomasi, J.; Barone, V.; Mennucci, B.; Cossi, M.; Scalmani, G.; Rega, N.; Petersson, G. A.; Nakatsuji, H.; Hada, M.; Ehara, M.; Toyota, K.; Fukuda, R.; Hasegawa, J.; Ishida, M.; Nakajima, T.; Honda, Y.; Kitao, O.; Nakai, H.; Klene, M.; Li, X.; Knox, J. E.; Hratchian, H. P.; Cross, J. B.; Bakken, V.; Adamo, C.; Jaramillo, J.; Gomperts, R.; Stratmann, R. E.; Yazyev, O.; Austin, A. J.; Cammi, R.; Pomelli, C.; Ochterski, J. W.; Ayala, P. Y.; Morokuma, K.; Voth, G. A.; Salvador, P.; Dannenberg, J. J.; Zakrzewski, V. G.; Dapprich, S.; Daniels, A. D.; Strain, M. C.; Farkas, O.; Malick, D. K.; Rabuck, A. D.; Raghavachari, K.; Foresman, J. B.; Ortiz, J. V.; Cui, Q.; Baboul, A. G.; Clifford, S.; Cioslowski, J.; Stefanov, B. B.; Liu, G.; Liashenko, A.; Piskorz, P.; Komaromi, I.; Martin, R. L.; Fox, D. J.; Keith, T.; Al-Laham, M. A.; Peng, C. Y.; Nanayakkara, A.; Challacombe, M.; Gill, P. M. W.; Johnson, B.; Chen, W.; Wong, M. W.; Gonzalez, C.; Pople, J. A. *Gaussian 03, Revision C.02*; Gaussian, Inc., Wallingford CT, **2004**.
(38) a) Becke, A. D. "Density-functional thermochemistry. III. The role of exact exchange" *J. Chem. Phys.* **1993**, *98*, 5648; b) Lee, C.; Yang, W.; Parr, R. G. "Development of the Colle-Salvetti correlation-energy formula into a functional of the electron density" *Phys. Rev. B* **1988**, *37*, 785; c) Becke, A. D. "Density-functional exchange-energy approximation with correct asymptotic behavior" *Phys. Rev. A* **1988**, *38*, 3098.
(39) a) Bos, J.; Garcia-Herraiz, A.; Roelfes, G. "An enantioselective artificial metallo-hydratase" *Chem. Sci.* **2013**, *4*, 3578; b) Basler, S.; Studer, S.; Zou, Y.; Mori, T.; Ota, Y.; Camus, A.; Bunzel, H. A.; Helgeson, R. C.; Houk, K. N.; Jiménez-Osés, G.; Hilvert, D. "Efficient Lewis acid catalysis of an abiological reaction in a de novo protein scaffold" *Nat. Chem.* **2021**, *13*, 231; c) Robles, V. M.; Dürrenberger, M.; Heinisch, T.; Lledós, A.; Schirmer, T.; Ward, T. R.; Maréchal, J.-D. "Structural, Kinetic, and Docking Studies of Artificial Imine Reductases Based on Biotin–Streptavidin Technology: An Induced Lock-and-Key Hypothesis" *J. Am. Chem. Soc.* **2014**, *136*, 15676.
(40) Alonso-Cotchico, L.; Rodríguez-Guerra, J.; Lledós, A.; Maréchal, J.-D. "Molecular Modeling for Artificial Metalloenzyme Design and Optimization" *Acc. Chem. Res.* **2020**, *53*, 896.
(41) Martins, Floriane L.; Pordea, A.; Jäger, C. M. "Computationally driven design of an artificial metalloenzyme using supramolecular anchoring strategies of iridium complexes to alcohol dehydrogenase" *Faraday Discussions* **2022**, *234*, 315.
(42) Villarino, L.; Splan, K. E.; Reddem, E.; Alonso-Cotchico, L.; Gutiérrez de Souza, C.; Lledós, A.; Maréchal, J.-D.; Thunnissen, A.-M. W. H.; Roelfes, G. "An Artificial Heme Enzyme for Cyclopropanation Reactions" *Angew. Chem. Int. Ed.* **2018**, *57*, 7785.
(43) Fujieda, N.; Ichihashi, H.; Yuasa, M.; Nishikawa, Y.; Kurisu, G.; Itoh, S. "Cupin Variants as a Macromolecular Ligand Library for Stereoselective Michael Addition of Nitroalkanes" *Angew. Chem. Int. Ed.* **2020**, *59*, 7717.
(44) Drienovská, I.; Alonso-Cotchico, L.; Vidossich, P.; Lledós, A.; Maréchal, J.-D.; Roelfes, G. "Design of an enantioselective artificial metallo-hydratase enzyme containing an unnatural metal-binding amino acid" *Chem. Sci.* **2017**, *8*, 7228.

(45) a) Karlsson, A.; Parales, J. V.; Parales, R. E.; Gibson, D. T.; Eklund, H.; Ramaswamy, S. "Crystal structure of naphthalene dioxygenase: Side-on binding of dioxygen to iron" *Science* **2003**, *299*, 1039; b) Kovaleva, E. G.; Lipscomb, J. D. "Crystal structures of Fe2+ dioxygenase superoxo, alkylperoxo, and bound product intermediates" *Science* **2007**, *316*, 453; c) Casadei, C. M.; Gumiero, A.; Metcalfe, C. L.; Murphy, E. J.; Basran, J.; Concilio, M. G.; Teixeira, S. C. M.; Schrader, T. E.; Fielding, A. J.; Ostermann, A.; Blakeley, M. P.; Raven, E. L.; Moody, P. C. E. "Neutron cryo-crystallography captures the protonation state of ferryl heme in a peroxidase" *Science* **2014**, *345*, 193; d) Huang, X.; Groves, J. T. "Oxygen Activation and Radical Transformations in Heme Proteins and Metalloporphyrins" *Chem. Rev.* **2018**, *118*, 2491.
(46) Miller, K. R.; Biswas, S.; Jasniewski, A.; Follmer, A. H.; Biswas, A.; Albert, T.; Sabuncu, S.; Bominaar, E. L.; Hendrich, M. P.; Moënne-Loccoz, P.; Borovik, A. S. "Artificial Metalloproteins with Dinuclear Iron–Hydroxido Centers" *J. Am. Chem. Soc.* **2021**, *143*, 2384.
(47) Mann, S. I.; Heinisch, T.; Ward, T. R.; Borovik, A. S. "Peroxide Activation Regulated by Hydrogen Bonds within Artificial Cu Proteins" *J. Am. Chem. Soc.* **2017**, *139*, 17289.
(48) Abe, S.; Maity, B.; Ueno, T. "Functionalization of protein crystals with metal ions, complexes and nanoparticles" *Curr Opin Chem Biol* **2018**, *43*, 68.
(49) Falkner, J. C.; Turner, M. E.; Bosworth, J. K.; Trentler, T. J.; Johnson, J. E.; Lin, T.; Colvin, V. L. "Virus Crystals as Nanocomposite Scaffolds" *J. Am. Chem. Soc.* **2005**, *127*, 5274.
(50) Abe, S.; Tsujimoto, M.; Yoneda, K.; Ohba, M.; Hikage, T.; Takano, M.; Kitagawa, S.; Ueno, T. "Porous Protein Crystals as Reaction Vessels for Controlling Magnetic Properties of Nanoparticles" *Small* **2012**, *8*, 1314.
(51) Abe, S.; Ueno, T. "Design of protein crystals in the development of solid biomaterials" *RSC Advances* **2015**, *5*, 21366.
(52) Sheldon, R. A.; Woodley, J. M. "Role of Biocatalysis in Sustainable Chemistry" *Chem. Rev.* **2018**, *118*, 801.
(53) Sheldon, R. A.; Schoevaart, R.; Van Langen, L. M. "Cross-linked enzyme aggregates (CLEAs): A novel and versatile method for enzyme immobilization (a review)" *Biocatalysis and Biotransformation* **2005**, *23*, 141.
(54) Doscher, M. S.; Richards, F. M. "The Activity of an Enzyme in the Crystalline State: Ribonuclease S" *J. Biol. Chem.* **1963**, *238*, 2399.
(55) Lopez, S.; Rondot, L.; Leprêtre, C.; Marchi-Delapierre, C.; Ménage, S.; Cavazza, C. "Cross-Linked Artificial Enzyme Crystals as Heterogeneous Catalysts for Oxidation Reactions" *J. Am. Chem. Soc.* **2017**, *139*, 17994.
(56) Tabe, H.; Abe, S.; Hikage, T.; Kitagawa, S.; Ueno, T. "Porous Protein Crystals as Catalytic Vessels for Organometallic Complexes" *Chem. Asian J.* **2014**, *9*, 1373.
(57) Tabe, H.; Takahashi, H.; Shimoi, T.; Abe, S.; Ueno, T.; Yamada, Y. "Photocatalytic hydrogen evolution systems constructed in cross-linked porous protein crystals" *Applied Catalysis B: Environmental* **2018**, *237*, 1124.